Ki-67 contributes to normal cell cycle progression and inactive X heterochromatin in p21 checkpoint-proficient human cells

Xiaoming Sun[1], Aizhan Bizhanova[1], Timothy D. Matheson[1], Jun Yu[1], Lihua Julie Zhu[1,2,3], Paul D. Kaufman[1,3,#]

[1]Department of Molecular, Cell and Cancer Biology
University of Massachusetts Medical School, Worcester, MA 01605, USA

[2]Program in Bioinformatics and Integrative Biology
University of Massachusetts Medical School, Worcester, MA 01605, USA.

[3]Program in Molecular Medicine
University of Massachusetts Medical School, Worcester, MA 01605, USA.

Running title: Ki-67 affects S phase entry and Xi heterochromatin

[#]Corresponding Author (paul.kaufman1@umassmed.edu)

Word count for Abstract: 197

Word count for the Materials and Methods section: 2437

Combined word count for the Introduction, Results, and Discussion: 4809

Abstract

Ki-67 protein is widely used as a tumor proliferation marker. However, whether Ki-67 affects cell cycle progression has been controversial. Here, we demonstrate that depletion of Ki-67 in human hTERT-RPE1, WI-38, IMR90, hTERT-BJ cell lines and primary fibroblast cells slowed entry into S phase and coordinately downregulated genes related to DNA replication. Some gene expression changes were partially relieved in Ki-67-depleted hTERT-RPE1 cells by co-depletion of the Rb checkpoint protein, but more thorough suppression of the transcriptional and cell cycle defects was observed upon depletion of cell cycle inhibitor p21. Notably, induction of p21 upon depletion of Ki-67 was a consistent hallmark of cell types in which transcription and cell cycle distribution were sensitive to Ki-67; these responses were absent in cells that did not induce p21. Furthermore, upon Ki-67 depletion, a subset of inactive X (Xi) chromosomes in female hTERT-RPE1 cells displayed several features of compromised heterochromatin maintenance, including decreased H3K27me3 and H4K20me1 labeling. These chromatin alterations were limited to Xi chromosomes localized away from the nuclear lamina and were not observed in checkpoint-deficient 293T cells. Altogether, our results indicate that Ki-67 integrates normal S phase progression and Xi heterochromatin maintenance in p21 checkpoint-proficient human cells.

INTRODUCTION

Ki-67 was first identified via an antibody raised against Hodgkin lymphoma cell nuclei (1). Because Ki-67 is generally expressed strongly in proliferating cells and poorly in quiescent cells (2), anti-Ki-67 antibodies are frequently used to detect proliferative cells in

50 clinical studies (3,4). In interphase cells, Ki-67 primarily localizes to the nucleolus (5-7),
51 whereas during mitosis, it coats the chromosomes (8-10). In the past few years, several
52 studies have greatly increased our understanding of Ki-67 function. This is particularly true
53 for its mitotic roles. Specifically, Ki-67 is required for formation of the mitotic
54 perichromosomal layer (11,12), a proteinaceous sheath that coats mitotic chromosomes
55 (13,14). As part of this layer, Ki-67's large size and highly positively-charged amino acid
56 composition keeps individual mitotic chromosomes dispersed rather than aggregated upon
57 nuclear envelope disassembly, thereby ensuring normal kinetics of anaphase progression
58 (15). At anaphase onset, Ki-67 binds protein phosphatase 1γ (PP1γ) to form a holoenzyme
59 (16) important for targeting substrates that must be dephosphorylated during mitotic exit
60 (10). In contrast to its structural role on the mitotic chromosomal surface, Ki-67 does not
61 appear to affect nucleosomal spacing (15) or condensation of individual mitotic
62 chromosomes (11,15).

63 In addition to its expression in proliferating cells, other experiments suggested Ki-
64 67 has a positive role in regulating cell proliferation. In early studies, antisense
65 oligonucleotides targeting Ki-67 expression in human IM-9 multiple myeloma cells blocked
66 [^{3}H]-thymidine incorporation, indicative of inhibition of proliferation (17). Likewise, Ki-67-
67 targeted phosphorothioate anti-sense oligonucleotides that resulted in partial depletion of
68 Ki-67 protein inhibited proliferation of human RT-4 bladder carcinoma and other tumor
69 cell lines (18). More recently, siRNA-mediated depletion of Ki-67 resulted in reduced
70 proliferation in human 786-0 renal carcinoma cells (19).

71 However, despite its utility as a proliferation marker, the contribution of Ki-67 to
72 cell proliferation has recently been questioned. For example, in one recent study, genetic

73 disruption of Ki-67 in human MCF-10A epithelial breast and DLD-1 colon cancer cells did
74 not affect cell proliferation rates in bulk culture, although clonogenic growth of highly
75 diluted cell populations was reduced (20). In another recent study, depletion of Ki-67 in
76 human HeLa or U2OS cells did not alter cell cycle distribution (12). These data raise the
77 possibility that Ki-67 function may have different consequences in different cell types.
78 In our previous studies we demonstrated that the interphase and mitotic
79 localization of Ki-67 is partially dispersed in cells lacking the N-terminal domain of the
80 p150 subunit of Chromatin Assembly Factor-1 (21, 22). We therefore began exploring the
81 functions of Ki-67 in several human cell types. Here, we show that the contribution of Ki-67
82 to cell proliferation depends on cell type. In hTERT-RPE1, WI-38, IMR90, and hTERT-BJ
83 cells and primary foreskin fibroblasts, depletion of Ki-67 resulted in reduced frequencies of
84 S-phase cells and concomitant reduction in S phase-related transcript levels. We show that
85 in female hTERT-RPE1 cells, these phenotypes required a p21 checkpoint-mediated delay
86 in S phase entry, and are accompanied by altered nucleolar association and chromatin
87 characteristics of the inactive X (Xi) chromosome. Notably, none of these phenotypes were
88 observed in human cells unable to induce p21 in response to Ki-67 depletion. Therefore, Ki-
89 67 is important for normal S phase progression in p21 checkpoint-proficient human cells,
90 in a manner correlated with its contribution to Xi heterochromatin composition.
91
92 RESULTS
93 **Ki-67 affects S phase gene expression and progression**
94 To explore how Ki-67 impacts gene expression, we performed RNAseq analyses of
95 control and Ki-67-depleted hTERT-RPE1 cells, a diploid retinal pigment epithelial cell line

96 immortalized by an hTERT transgene (23). Duplicate analyses were highly reproducible
97 (Figures 1A-B). Ki-67 depletion resulted in approximately equal numbers of reduced and
98 increased RNA levels across the transcriptome (Figure 1C). However, Reactome pathway
99 analysis of RNA abundance changes showed that the most altered functional sets of genes
100 included those involved in DNA replication and cell cycle progression (Figure 1D). For
101 example, levels of RNAs encoding all subunits of several protein complexes involved in S
102 phase progression were concertedly reduced, including DNA replication clamp loader RFC
103 (RFC1-5 genes), ssDNA-binding complex RPA (RPA1-3), the replicative helicase (MCM1-6),
104 the GINS replication initiation complex (GINS1-4), the DNA polymerase alpha/primase
105 complex, as well as the DNA replication clamp PCNA and the flap-endonuclease FEN1
106 involved in Okazaki fragment maturation (Supplemental Tables 1-2). We confirmed
107 reduced levels of a subset of replication-related RNA targets by RT-qPCR analyses (Figures
108 1E-F). Notably, the RT-qPCR data were very similar when obtained with two distinct Ki-67
109 depletion reagents, one a synthetic siRNA and the other a cocktail of in vitro-diced dsRNAs
110 non-overlapping the siRNA target, both of which efficiently depleted steady-state Ki67
111 levels (Figures 1M-N).
112 We also observed that fluorescence-activated cell sorting (FACS) analysis of Br-
113 dUTP-labeled cells showed that the proportion of S phase cells decreased upon depletion of
114 Ki-67 in hTERT-RPE1 cells with either depletion reagent (Figure 1G-H; quantified in Fig. 1I
115 and 1K). In contrast, proportions of G1 and G2/M populations were not significantly
116 altered (Fig. 1J and 1L). Therefore, Ki-67 is important for normal S phase distribution and
117 gene expression in hTERT-RPE1 cells.

118 As an additional control for the direct effect of the siRNA treatment, we used
119 CRISPR/Cas9 to mutate the siRNA target site in hTERT-RPE1 cells (Fig. 2A-B). In a resulting
120 homozygous mutant cell line (Figure 2C), siKi-67 no longer depleted Ki-67 protein levels,
121 but as expected the esiKi-67 reagent was still effective (Figure 2D). We also observed that
122 siKi-67 no longer altered candidate S phase RNA levels in the resistant cell line, but esiKi-
123 67 did (Figure 2E). We conclude that the transcriptional response to acute depletion of the
124 Ki-67 mRNA is due to loss of Ki-67 protein.
125 However, recent studies challenge the view that Ki-67 is important for human cell
126 proliferation; for example, depletion of Ki-67 had minimal effects on the cell cycle
127 distribution of tumor-derived HeLa or U2OS cells (12). Because our data indicated that Ki-
128 67 contributes to normal cell cycle progression in hTERT-RPE1 cells, we hypothesized that
129 the contribution of Ki-67 to cell cycle progression would be cell type-dependent, and may
130 be related to checkpoint function. To explore this idea, we depleted Ki-67 in several
131 additional cell lines. We compared diploid, non-immortal WI-38 and IMR90 fibroblasts,
132 hTERT-immortalized BJ fibroblasts, and primary human foreskin fibroblasts (HFFs) with
133 tumor-derived cell lines: virally-transformed kidney (293T) or cervical carcinoma (HeLa)
134 cells, and osteosarcoma U2OS cells. Importantly, we confirmed that all these cells could be
135 efficiently depleted of Ki-67 protein using both of our depletion reagents (Figure 2F-L).
136 In all of the experiments with the non-tumor-derived cells, we observed reduced
137 replication factor RNA levels and fewer cells in S phase, similar to our results in hTERT-
138 RPE1 cells, and these results were independent of which Ki-67 depletion reagent was used
139 (Figures 3-4). In contrast, in the tumor-derived cell lines, Ki-67 depletion did not result in
140 uniform down regulation of the S phase genes tested, nor were there changes in cell cycle

141 distribution (Figures 5-6). These data are consistent with RNAseq data sets in HeLa and
142 U2OS cells (12) that did not display concerted downregulation of DNA replication genes.
143 We conclude that the effects of Ki-67 depletion on RNA levels and cell cycle distribution are
144 cell type-dependent.

145 The FACS analyses of asynchronous cell populations indicated that Ki-67 depletion
146 most significantly affects S phase in the sensitive cell types. To examine this in more detail,
147 we analyzed the kinetics of DNA synthesis in synchronized hTERT-RPE1 cells. Cells were
148 blocked near the G1-S transition of the cell cycle with hydroxyurea (HU) for 15 hours
149 (Figure 7A) (24), which provided efficient arrest (Fig. 7D). Cells were then released into
150 drug-free media and pulse-labeled with the deoxynucleotide analog EdU at two-hour
151 timepoints across an 8-10-hour time course. In control cells treated with the scrambled
152 siRNA, EdU labeling was first detected at the 2 hour time point, and displayed a typical
153 early S phase pattern consisting of many small foci (25). At later time points, the pulse of
154 EdU labeled larger foci, indicative of mid-late S phase patterns. Upon Ki-67 depletion, we
155 observed a delay in the initial detection of EdU incorporation of approximately 2 hours
156 (Figure 7B). Notably, the Ki-67-depleted population also displayed a higher percentage of
157 cells that did not incorporate EdU during the time course (Figure 7C). Together, these data
158 are consistent with our transcriptomic and FACS data indicating that Ki-67 depletion
159 affects S-phase in hTERT-RPE-1 cells (Figure 1).

160

161 **Checkpoint responses to Ki-67 depletion**

162 Because Ki-67 depletion did not affect S phase transcription or cell cycle
163 progression in tumor-derived cell lines, our data suggested that functional checkpoints are

164 required for sensitivity to Ki-67 depletion. Consistent with this idea were comparisons of
165 our RNAseq data with metadata analyses of genes regulated by cell cycle status or by E2F
166 transcription factors (26) that are important for G1/S cell cycle phase transcription (26-
167 28). These meta-analyses aggregated multiple datasets, finding that similar results in
168 multiple datasets strongly predicted regulatory network connections that could be missed
169 in single experiments. Of the cell cycle-regulated genes identified in that study, we find
170 those that peak during G1/S phase were more frequently downregulated than upregulated
171 upon Ki-67 depletion (Fig. 8A; Supplemental Table 3). Consistent with this observation,
172 E2F target RNA levels (Fig. 8B) were much more frequently downregulated than
173 upregulated upon Ki-67 depletion. These comparisons were consistent with the idea that
174 checkpoint activation contributed to the observed delay in S phase entry and
175 transcriptional phenotypes in Ki-67-depleted cells.
176 To test this, we performed experiments co-depleting checkpoint proteins. First, we
177 took advantage of a derivative of hTERT-RPE1 cells that have an integrated, doxycycline-
178 inducible shRNA that targets the RB mRNA (29). Rb levels remained unchanged in these
179 cells in the absence of doxycycline (Fig. 8C), and siRNA-mediated depletion of Ki-67
180 resulted in reduced S phase-related RNA levels as was observed previously (Fig. 8D).
181 Addition of doxycycline to deplete Rb, together with a control scrambled siRNA leaving Ki-
182 67 levels unchanged, did not significantly alter S-phase related target RNA levels (Fig. 8D).
183 In contrast, simultaneous depletion of Rb and Ki-67 resulted in RNA levels at two of the
184 four loci tested that were significantly elevated compared to those in cells depleted of Ki-67
185 alone (Fig. 8D). FACS analysis indicated that Rb depletion was insufficient to significantly

186 change the cell cycle profile of Ki-67-depleted cells (Fig. 8E-F). We conclude that depletion
187 of Rb only partially relieves the cellular response to Ki-67 depletion in hTERT-RPE1 cells.
188 Therefore, we reasoned other factors must contribute. One clue was provided by
189 comparison of the si-Ki-67 RNAseq data to metadata analysis of binding by subunits of the
190 transcription repressor complex termed DREAM (26). We observed that genes with the
191 highest predicted probability of DREAM binding were very frequently downregulated upon
192 Ki-67 depletion (Fig. 8G). In mammalian cells, DREAM is a master regulator of cell cycle-
193 dependent gene expression, repressing both G1/S and G2/M targets, and gene repression
194 by DREAM requires the p21 checkpoint protein (27,30,31). p21 is a potent universal CDK
195 inhibitor (CKI). During G1 and S phases, p21 directly binds to and inhibits the kinase
196 activity of cyclin E-CDK2, cyclin B1-CDK1 and cyclin D-CDK4/6 complexes (32-34).
197 Furthermore, p21 also directly inhibits DNA synthesis by binding to PCNA, the sliding
198 clamp required for processive DNA polymerase activity (35). Therefore we hypothesized
199 that p21 could be important for the response to Ki-67 depletion (Figure 8H).
200 Consequently, we next tested effects of Ki-67 depletion the *CDKN1A* gene, which
201 encodes p21. Our RNAseq data indicated increased *CDKN1A* RNA levels in Ki-67 depleted
202 hTERT-RPE1 cells (log2 fold change = +0.48, $p = 0.016$), although multiple hypothesis
203 testing indicated that these values did not achieve the stringent statistical significance
204 cutoff of $q < 0.05$ (Supplemental Table 2). RT-PCR measurements of *CDKN1A* RNA levels
205 demonstrated a significant increase in four diploid cell types, but not in 293T cells (Fig.
206 9A). We note that induction of *CDKN1A* RNA was dependent on having an intact siRNA
207 target site in the Ki-67 gene, indicating this is a direct effect of Ki-67 depletion (Figure 2E).

208 Consistent with the increased RNA levels, we detected elevated p21 protein levels in
209 hTERT-RPE1 but not 293T cells (Fig. 9B).
210 p21 is a direct target of transcriptional induction by the tumor suppressor p53, and
211 the cell lines examined thus far therefore implicated active p53 in the sensitivity to Ki-67
212 (36,37). To examine this relationship further, we compared the effects of Ki-67 depletion in
213 additional cancer cell lines, including two expressing wild-type p53, MCF7 and HCT116,
214 and also MDA-MB-231 cells which express a mutant p53 defective for p21 induction (38).
215 In MCF7 breast adenocarcinoma cells, we observed that Ki-67 depletion elevated p21 RNA
216 and protein levels (Fig. 9 G,H), and down-regulated replication-related RNAs (Fig. 9H). In
217 contrast, in HCT116 colorectal carcinoma and MDA-MB-231 breast adenocarcinoma cells,
218 Ki-67 depletion did not increase p21 expression or cause concerted down-regulation of S
219 phase genes (Fig. 9G, I, J). Because HCT116 and MDA_MB-231 cells differ in their p53
220 status, we conclude that p53 status cannot always predict the response to Ki-67 depletion.
221 Instead, we find that induction of p21 upon Ki-67 depletion is a consistent hallmark of this
222 form of checkpoint activation.
223 To assess the functional consequence of p21 induction, we performed co-depletion
224 experiments in hTERT-RPE1 cells (Fig. 9D). We observed that cells simultaneously
225 depleted of both Ki-67 and p21 no longer displayed the reduced levels of any of the four S
226 phase-related mRNAs analyzed (Fig. 9D). Furthermore, FACS analysis of the co-depleted
227 cells showed that there was significant restoration of the percentage of cells in S phase
228 upon codepletion of p21 with Ki-67 (Fig. 9E-F). We conclude that induction of p21 is
229 functionally important for the effects of Ki-67 depletion on cell cycle distribution in hTERT-
230 RPE1 cells.

231 **Ki-67 affects heterochromatic characteristics of the inactive X chromosome**

232 Ki-67 is required for the normal cellular localization of heterochromatin-associated
233 histone modifications (12), and for the interphase nucleolar association of heterochromatic
234 loci(22). Because the inactive X (Xi) chromosome is a well-studied example of facultative
235 heterochromatin that associates with the nucleoli of female mouse (24) and human cells
236 (39-41), we tested whether Ki-67 affected characteristics of Xi heterochromatin. Indeed, Ki-
237 67 depletion in hTERT-RPE1 cells resulted in a subset of cells that displayed reduced
238 staining intensity for antibodies recognizing H3K27me3 and H4K20me1, histone
239 modifications that are enriched on the Xi (42,43)(Figure 10A, C, E, G). H3K27me3 is
240 generated by the Polycomb PRC2 complex and is a keystone of facultative heterochromatic
241 silencing (44-46). H4K20me1 is generated by the PR-Set7/Set8/KMT5a enzyme (47) and
242 together with H3K27me3 is an early mark on Xi chromosomes during the process of XIST-
243 mediated inactivation (43,47). Notably, changes to either of these histone modifications
244 were only observed in cells in which the Xi was localized away from the nuclear periphery
245 (Fig. 10B, D, F, H). Furthermore, these changes were not observed in 293T cells that also
246 lacked the cell cycle response to Ki-67 depletion (Fig. 11). Therefore, the response of
247 hTERT-RPE1 cells to Ki-67 depletion involves two classes of correlated events that are both
248 absent in 293T cells: checkpoint-mediated perturbation of S phase, and altered Xi
249 heterochromatin.

250 Increased levels of repetitive element-rich Cot-1-hybridizing transcripts and RNA
251 polymerase II have previously been observed in breast cancer cell lines that display
252 perturbations in Xi chromatin (48). We tested for changes in these properties as well, and
253 we detected an increase in the frequency of cells that display Cot-1-hybridizing transcripts

254 or RNA polymerase II on the Xi upon Ki-67 depletion in hTERT-RPE1 cells (Figures 12-13).
255 As observed above for the histone modifications (Fig. 10), increased levels of Cot-1 RNA
256 and Pol II within the XIST domain were only observed in cells in which the Xi was localized
257 away from the nuclear periphery. Also, as for all other phenotypes detected, these changes
258 were similar with either Ki-67 depletion reagents (Figs. 12-13).
259 However, not all aspects of Xi heterochromatin were sensitive to Ki-67 depletion.
260 For example, Ki-67 depletion did not alter the overall appearance of the XIST "cloud" that
261 covers the Xi (Fig. 14A). In addition, RT-PCR showed no significant down regulation of
262 XIST transcript expression (Fig. 10J). Also, there was no evidence for Xi chromosome-wide
263 deprepression of transcription, as shown in the analysis of X-linked gene expression (Fig.
264 14B), or in the analysis of allele-specific transcription of X-linked genes detected via
265 analysis of known SNPs (Supplemental Table 4). Furthermore, an additional mark
266 associated with the Xi, the histone variant macroH2A, did not change in appearance upon
267 depletion of Ki-67 (Fig. 14C-H). Together, the Xi data indicate that acute depletion of Ki-67
268 alters several, but not all, characteristics of Xi heterochromatin in hTERT-RPE1 cells.
269 Importantly, changes in H3K27me3 and H4K20me1 staining were not observed in 293T
270 cells, indicating a correlation between checkpoint activation and effects on the Xi upon Ki-
271 67 depletion.
272
273 **Ki-67 affects the S phase nucleolar association of the inactive X chromosome**
274 The perinucleolar space is a subset of the heterochromatic compartment; another
275 frequent location for heterochromatin is at the nuclear periphery, adjacent to the nuclear
276 lamina (49). Accordingly, the Xi is usually localized to one of these two preferred locations

277 (24). However, heterochromatic sequences can dynamically relocalize from nucleoli to the
278 periphery, either during cell division or upon perturbing the nucleolus with actinomycin
279 (49-52). Because Ki-67 depletion affected heterochromatic marks only on Xi chromosomes
280 away from the nuclear periphery (Figs. 10-13), we hypothesized that it might also affect the
281 interphase localization of the Xi. We first examined Xi localization in asynchronous hTERT-
282 RPE1 cells, using immuno-RNA-FISH to detect Xi-associated lncRNA XIST and nucleolar
283 protein fibrillarin. Indeed, Ki-67 depletion resulted in a partial but statistically significant
284 reduction in Xi-nucleolar associations (Figure 15A-D). This loss of nucleolar association
285 was accompanied by an increase of similar magnitude in Xi-lamina associations, and
286 similar results were observed with our two distinct Ki-67 depletion reagents (Figures 15B,
287 D). However, in 293T cells, we observed no significant alteration in Xi-nucleolar
288 associations (Fig. 15E-H). Thus, distribution of the Xi within the interphase nucleus is
289 sensitive to Ki-67 depletion in a cell type that induces p21.

290 Previous studies in mouse cells showed that the Xi-nucleolar association is cell-cycle
291 regulated, occurring most prevalently in S phase cells (24). Therefore, we examined Xi
292 localization in hTERT-RPE1 cells prepared in the same manner as in the cell
293 synchronization experiments in Figure 7A-B. Consistent with published data from mouse
294 cells (24), the frequency of Xi-nucleolar associations peaked in middle S-late S phase
295 transition; this was true for the frequency of Xi associations that were exclusively at the
296 nucleolus (Fig. 15I), and for the frequency of Xi chromosomes simultaneously associated
297 with both the nucleolus and the lamina (Fig. 15J). These peaks occurred in both the control
298 and Ki-67-depleted populations, with the Xi-nucleolar interaction peaks delayed two hours

299 in the latter case. The two-hour shift correlates with the delay in S phase entry in the Ki-67-
300 depleted cells (Fig. 7).
301 As suggested by the Xi localization data from asynchronous cells (Fig. 15A-D), Xi
302 associations with the nucleoli and lamina were inversely related, so that the peak of
303 nucleolar associations (Figure 15I-J) coincided with the lowest frequencies of laminar
304 associations (Fig. 15K). We note that when the total Xi-laminar association frequencies
305 were counted by summing the exclusively laminar associations (Fig. 15K) plus those also
306 associated with nucleoli simultaneously (Fig. 15J), we observed little change during the
307 experiment (Figure 15L). Thus, the biggest changes during S phase are lamina-associated Xi
308 becoming transiently also associated with nucleoli (e.g. compare Fig. 15J and 15K).
309 Together, these data indicated that cell cycle-regulated Xi-nucleolar associations are
310 delayed in concert with DNA synthesis upon depletion of Ki-67 in hTERT-RPE1 cells. Thus,
311 checkpoint activation upon Ki-67 depletion affects cell cycle progression and gene
312 expression, and these effects are correlated with altered Xi heterochromatin in female
313 hTERT-RPE1 cells.
314

315 **Discussion**
316
317 **Cell-type specific responses to Ki-67 depletion**

318 Our studies show that Ki-67 expression is important for normal S phase progression
319 in primary human foreskin fibroblasts, non-transformed fibroblast lines (WI-38 and
320 IMR90), hTERT-immortalized BJ fibroblasts, and hTERT-immortalized RPE1 cells (23), a
321 human female retinal pigment epithelial cell line with a diploid karyotype (53). In contrast,
322 in cancer-derived 293T, U2OS and HeLa cells, depletion of Ki-67 did not cause defects in

323 cell proliferation. Therefore, we conclude that Ki-67 is required for normal cell cycle
324 progression in some but not all cell lines. Our data distinguish two types of responses to
325 depletion of Ki-67 in human cells, depending on whether cells are able to mount a p21-
326 dependent checkpoint.

327 hTERT-BJ fibroblasts were sensitive to Ki-67 depletion in our assays; however, a
328 previous study indicated that shRNA-mediated Ki-67 depletion did not affect hTERT-BJ cell
329 cycle re-entry after starvation (12). Therefore, not all assays can detect the effects of Ki-67
330 depletion. For example, two assays used in the previous study are insensitive to the cell
331 cycle progression delays that we observe upon Ki-67 depletion. First, one-dimensional flow
332 cytometry of propidium iodide-stained asynchronous populations cannot detect the S
333 phase delays we detect in BrdU labeling experiments; second, a 3 hour EdU pulse is too
334 long to capture the 2-hour S phase entry delay. Together, our data indicate that the effects
335 of Ki-67 on S phase progression are transient in sensitive cell types and therefore most
336 easily observed using short pulses of labeled deoxynucleotides.

337

338 **Characteristics of checkpoint activation caused by Ki-67 depletion**

339 Meta-analyses of our RNAseq data showed that Ki-67 depletion in hTERT-RPE1 cells
340 resulted in frequent repression of Rb/E2F-regulated, G1/S expressed genes. However,
341 depletion of the Rb checkpoint protein only partially relieved transcriptional repression
342 and did not restore normal percentages of S phase cells, indicating that additional factors
343 were responsible for the altered cell cycle profile in Ki-67 depleted cells.

344 A strong candidate for such a factor is the DREAM complex, which represses G1/S-
345 expressed cell cycle genes in a p21-dependent manner (26, 54). We noticed frequent

346 downregulation of DREAM complex targets in Ki-67-depleted cells, which lead us to test
347 whether sensitivity to Ki-67 depletion was also p21-dependent. Notably, both the
348 transcriptional alterations and cell cycle perturbations caused by Ki-67 depletion were
349 partially relieved by simultaneous depletion of p21. Importantly, cell lines that induce p21
350 upon Ki-67 depletion are those that inhibit transcription of DNA replication genes and
351 delay entry into S-phase. Thus, this study implicates a p21-dependent checkpoint in cells
352 sensitive to Ki-67 depletion.

353 A recent study shows that PD0332991, a small molecule CDK4/CDK6 inhibitor
354 (CDKi), depletes Ki-67 protein levels in some but not all cell lines (55). In "CDKi-sensitive"
355 cells, this compound causes G1 cell cycle arrest via an Rb-mediated checkpoint, inhibiting
356 Ki-67 and cyclin A gene transcription while proteasome-mediated degradation destroys
357 existing Ki-67 protein molecules. CDKi-sensitivity appears similar to many of the responses
358 we observe upon Ki-67 depletion, and CDKi-sensitive cells include IMR90 and primary
359 fibroblasts that we found to be "Ki-67 sensitive". MCF7 breast adenocarcinoma cells are
360 also CDKi-sensitive (55), and we find that upon Ki-67 depletion MCF7 cells induce p21 and
361 down-regulate DNA replication genes. In contrast, HeLa and U2OS cells are not sensitive to
362 either CDKi or Ki-67 depletion. Thus, depletion of Ki-67 via CDKi treatment (55) or via
363 siRNA (this work) often leads to similar outcomes.

364 However, there is a counterexample to these correlations. CDKi treatment blocks S
365 phase entry and depletes Ki-67 in MDA-MB-231 breast adenocarcinoma cells (55). In
366 contrast, upon Ki-67 depletion, MDA-MB-231 cells did not display either p21 induction or
367 transcriptional down-regulation of S phase genes. Therefore, proteasome-mediated
368 degradation of Ki-67 via CDK4/6 inhibition is not equivalent to siRNA-mediated Ki67

369 depletion in all cell types. We hypothesize that a key difference is related to induction of
370 p21 in "Ki-67-sensitive" cell lines. p21 contributes to G1/S arrest via multiple mechanisms.
371 As a CDK inhibitor (32,33), p21 blocks CDK-mediated Rb phosphorylation thereby
372 inhibiting E2F-driven transcription(56). Likewise, it maintains activity of the
373 transcriptionally repressive DREAM complex which contain Rb-related p107/p130 "pocket
374 protein" subunits (26,27,54). p21 also directly interacts with PCNA and directly inhibits
375 DNA synthesis (35). Therefore, the lack of p21 induction in MDA-MD-231 cells may be the
376 key factor explaining the lack of "Ki-67 sensitivity" in this cell line. Future experiments will
377 be required to determine whether the activation of the DREAM complex or direct inhibition
378 of DNA synthesis machinery is more important for the "Ki-67-sensitive" phenotype
379 associated with p21 induction.
380 Regarding the defect in p21 induction in MDA-MB-231 cells, we note that they
381 express a gain-of-function R280K allele, which dominantly blocks p21 induction (38). Thus,
382 p53 status is likely a critical aspect of the different cell cycle responses to Ki-67 depletion in
383 many cell lines. However, sensitivity to Ki-67 depletion cannot always be predicted strictly
384 by p53 status. For example, HCT116 cells express wild-type p53 (38) but are not sensitive
385 to the CDKi PD0332991 (55), or to Ki-67 depletion (Fig. 9J). Because Ki-67 expression
386 predicts the differential response of different cell lines to CDKi treatment during xenograft
387 tumor formation (55), understanding how different checkpoint mutations alter Ki-67
388 expression and sensitivity to its depletion are important goals for developing stratified
389 approaches to cancer therapies.
390
391 **Ki-67 contributes to the interphase localization of the Xi chromosome**

392 Nucleoli are non-membrane bound organelles within the nucleus. Not only are these
393 sites of synthesis and assembly of ribosome components, the periphery of these organelles
394 plays an important role in higher order chromosome localization (49,57). Specifically, the
395 nucleolar periphery houses a subset of the cellular heterochromatin, which exchanges
396 dynamically with lamina-associated heterochromatin (50-52). Like other heterochromatin
397 regions, high resolution analysis of nucleolus-associated domains (termed NADs) in human
398 cells reveals enrichment of satellite repetitive DNAs and repressive histone marks
399 (51,58,59). Major questions in chromosome biology are how heterochromatin regions are
400 partitioned to different intranuclear locations, and how these interactions are governed by
401 cell cycle progression.
402 As a region of facultative heterochromatin, the Xi chromosome in female cells is
403 enriched in NAD loci, usually localized to either the nucleolar periphery or to the nuclear
404 lamina (24,40,58) . In mouse cells, the Xi-nucleolar association is cell cycle-dependent, with
405 frequencies peaking during mid-to-late S phase. A genetic deletion was used to show that
406 the long non-coding RNA Xist, which is expressed from the Xi chromosome, is required for
407 normal Xi-perinucleolar localization. Deletion of Xist results in diminished H3K27me3
408 enrichment and increased synthesis of Cot-1-hybridizing, repeat-derived RNAs on the Xi
409 (24). These data suggest that perinucleolar localization of Xi contributes to the
410 maintenance of heterochromatin structure. More recently, depletion of long non-coding
411 RNA Firre was shown to reduce association of the Xi to nucleolus in mouse cells, and also
412 reduces H3K27me3 density on the Xi (60). However, *Firre* depletion has minimal effects on
413 Xi gene silencing, consistent with the idea that multiple functionally overlapping factors
414 affect Xi heterochromatin localization and gene silencing.

415 Here, we discovered that Ki-67 affects the Xi-nucleolus interaction. Analysis of
416 synchronized RPE-1 cells shows that the association appears more slowly in Ki-67-
417 depleted cells, coincident with the delay in S phase entry. In addition to this delay, Ki-67
418 depletion alters some of the heterochromatin characteristics of the Xi, causing significantly
419 increased levels of Cot-1-hybridizing RNAs and Pol ll, and decreased enrichment of
420 H3K27me3 and H4K20me1. This loss of heterochromatic properties is partial in the cell
421 population, and we do not detect uniform reactivation of Pol II genes on the Xi. These data
422 are consistent with previous studies showing that multiple overlapping mechanisms
423 maintain the inactive status of the Xi (60,61). We note that XIST levels are not reduced
424 upon Ki-67 depletion (Supplemental Table 2; Fig. 10), suggesting that altered XIST levels
425 are unlikely to explain the effect of Ki-67 on the Xi. Instead, our data is consistent with the
426 view that Ki-67 is one of the factors that contributes to the maintenance of heterochromatic
427 structures of the Xi (12) in this case in a manner coupled to S phase progression.
428 Recent data show that the nuclear lamina localization mediated by the interaction
429 between XIST and the lamina B receptor facilitates the spreading of XIST on the Xi
430 chromosome, which in turn contributes to transcriptional silencing (62). This raises the
431 question of whether there are specific protein factors that contribute to the association of
432 the Xi with the nucleolus in addition to the lncRNAs XIST and FIRRE (24,60). Could Ki-67 be
433 such a factor? In support of this idea, Ki-67 is also required for association of other
434 heterochromatic regions with nucleoli in interphase cells (11,12,22).
435 It appears that the erosion of heterochromatic features on the Xi occurs in a
436 significant fraction of Ki-67-depleted cells away from the nuclear lamina, but the lamin-
437 associated Xi chromosomes are not altered. There are two possibilities to explain these

438 data. First, it may be that lamina association confers protection from heterochromatin
439 changes. Alternatively, Xi chromosomes that are most severely affected by Ki-67 depletion
440 may preferentially relocalize away from the lamina. Because our shRNA-based experiments
441 necessitate a 72-hour period to achieve strong Ki-67 depletion, there is likely passage
442 through multiple mitoses for each cell during this period. As Ki-67 is a key component of
443 the perichromosomal layer that envelopes each mitotic chromosome (11,15), it is tempting
444 to speculate that the loss of Ki-67 affects the reassociation of heterochromatic sequences
445 with the nuclear lamina or nucleoli after mitotic exit.
446

447 **Materials and Methods**

448 **Antibodies and Immunoblotting**

449 The following antibodies were used in this work:
450 rabbit anti-Ki-67 (Abcam Ab15580)
451 mouse anti-beta-tubulin (Ubpbio Y1060)
452 rabbit anti-fibrillarin (Abcam ab5821-100)
453 mouse anti-BrdU antibody (MoBu-1) (Abcam ab8039)
454 mouse anti-p21 antibody (Abcam ab109520)
455 rabbit anti-mcroH2A.1 (Abcam ab37264)
456 mouse anti-Rb antibody (4H1) (Cell signaling 9309)
457 mouse anti-H4K20Me1 (Active motif 39727)
458 mouse anti-RNA polymerase II, clone CTD4H8 (Millipore 05-623)
459 mouse anti-nucleophosmin (Santa Cruz Biotechnology sc-32256)
460 rabbit anti-WSTF (Cell signaling 2152)

461 rabbit anti-H3K27Me3 (Active motif 39535)

462

463 Amersham ECL Rabbit IgG, HRP-linked whole Ab (GElifescience NA934)

464 Donkey anti-Rabbit IgG (H+L) Secondary Antibody, Alexa Fluor® 594 (Life Technologies A-

465 21207)

466 Donkey anti-Rabbit IgG (H+L) Secondary Antibody, Alexa Fluor® 488 (Life Technologies

467 A-21206)

468 Streptavidin, Alexa Fluor® 488 Conjugate (Invitrogen S-32354)

469 DyLight 594 Labeled Anti-Digoxigenin/Digoxin (Vector Labs DI-7594)

470 For immunoblotting, cells were collected 3 days after RNAi transfection. Whole-cell lysates

471 were extracted in 20 mM Tris-HCl 7.5, 1% SDS and 10% glycerol supplemented with

472 protease inhibitor cocktail (Sigma P8340-1ml). The lysates were sonicated in a Bioruptor

473 set on high power for one 5 min cycle, with 30s on/30s off. 15 μg of each lysate were

474 separated by SDS-PAGE, transferred to PVDF membrane and probed as described in the

475 figure legends.

476

477 **Cell Cultures**

478 hTERT-RPE1 cells (a kind gift from Dr. Judith Sharp) and hTERT-BJ were cultured in

479 DMEM-F12 medium (VWR 12001-600) with 10% fetal bovine serum (FBS, Hyclone

480 #SH30910.03), 1% penicillin/streptomycin, 5% L-glutamine and 7.5% sodium bicarbonate

481 solution.

482 HeLa and U2OS cells were propagated in DMEM medium supplemented with 10% fetal

483 bovine serum. Cells were maintained > 25% confluence and passaged every three days.

484 Human foreskin fibroblasts (HFF, a kind gift from Dr. Jennifer Benanti, University of
485 Massachusetts Medical School (63) were maintained in DMEM containing 10% FBS and
486 antibiotic/antimycotic solution. HFF cells were grown at >25% confluence and were split
487 1:4 every 2 days. All cells were maintained in a 37 ^{0}C incubator with 5% CO_2.
488 WI-38 cells were maintained in DMEM and supplemented with 10% FBS, 2 mM L-
489 glutamine and antibiotic/antimycotic solution (Life Technologies, Carlsbad, CA). WI-38
490 cells were grown at >25% confluence and were split 1:4 every 2 days.
491 IMR-90 and MDA-MB-231 were maintained in DMEM medium with 10% FBS, 2mM L-
492 glutamine, and antibiotic/antimycotic solution. The cells were cultured at >25% confluence
493 and were split every 2 days.
494 HCT 116 (a kind gift of Dr. Anastassiia Vertii, University of Massachusetts Medical School)
495 and 293T cells were cultured in DMEM medium with 10% FBS. The cells were split 1:4
496 every 3 days
497 MCF7 cells were grown in RPMI medium with 10% FBS. The cells were split 1:3 every 3
498 days.
499 For hydroxyurea treatment, hTERT-RPE1 cells were cultured in the presence of 2 mM
500 hydroxyurea for 15 h, then washed with three times phosphate-buffered saline (PBS) and
501 released into hydroxyurea-free medium and harvested at the indicated time points.
502
503 **sgRNA design**
504 For editing the siRNA target site in the endogenous Ki-67 locus, four highest scoring single
505 guide RNAs (sgRNAs) targeting nucleotides 9661-9722 of the genomic DNA (NG_047061)

506 were selected by using the CRISPR Design web tool at http://crispr.mit.edu/ (64). The

507 sgRNA sequences are shown below:

508 5'-ACGTGCTGGCTCCTGTAAGT-3' (antisense)

509 5'-TCTAGCTTCTCTTCTGACCC-3' (sense)

510 5'-GATCTTGAGACACGACGTGC-3' (antisense)

511 5'- CTTCTGACCCTGGTGAGTAG-3' (sense)

512 These were cloned into a variant of the pX330 plasmid (64) with a puromycin-resistance

513 cassette (a kind gift from Kurtis McCannell and Dr. Thomas Fazzio, University of

514 Massachusetts Medical School) as previously described (65). To determine the most

515 efficient sgRNAs, 293T cells were transfected with FuGENE HD (Promega, catalog number

516 E2311) according to manufacturer's instructions. 500 ng of sequence-verified CRISPR

517 plasmid (pSpCas9-sgRNA) was transfected into 200×10^3 cells in 24 well dish. 48 hours

518 post-transfection, DNA was extracted using QuickExtract DNA extraction solution

519 (Epicentre, catalog number QE09050) according to manufacturer's instructions. Genomic

520 DNA was PCR amplified using a *Taq* DNA Polymerase (New England Biolabs, catalog

521 number M0273). The following primers were used for PCR amplification:

522 F2 primer: GGGTTCCAGCAATTCTCCTG

523 R primer: TCACCAAGGGAAAGTTAGGC

524 514 bp PCR products were ran on agarose gel and purified using Zymoclean Gel DNA

525 recovery kit (Zymo Research, catalog number D4007) and sent for Sanger sequencing at

526 Genewiz sequencing facility. The following primer was used for sequencing:

527 F primer: GCCAGGCTGTTCTCAAACTC

528 To assess gene editing in 293T cells by four sgRNA plasmids, TIDE web tool at https://tide-
529 calculator.nki.nl/ was used (66). Trace data for PCR fragment from GFP-transfected 293T
530 cells were used as a control sample chromatogram, and trace data for PCR fragments from
531 CRISPR plasmid-transfected cells were used as test sample chromatograms. The following
532 sgRNA was selected due to its efficiency in cutting and proximity to the siRNA site:
533 5'-GATCTTGAGACACGACGTGC-3' (referred to as sgKi-67 from now on).
534

535 **Co-transfection of CRISPR plasmid and HDR template into hTERT-RPE1 cells**

536 An HDR repair template carrying the siRNA-resistance conferring mutations, EcoO109I site
537 and 700 bp homology flanks on each side was purchased as a gBlock from Integrated DNA
538 Technologies. The template was cloned into pCR2.1 (Thermo Fisher Scientific, catalog
539 number K200001) according to manufacturer's instructions.
540 The sgKi-67 was cloned into a variant of the pX330 plasmid(64) with a neomycin-
541 resistance cassette (a kind gift from Kurtis McCannell and Dr. Thomas Fazzio, University of
542 Massachusetts Medical School) to facilitate gene editing in hTERT-RPE1. 3.3 μg of a 1:1
543 (v/v) mix of repair template and CRISPR plasmid were transfected using FuGENE HD into
544 75 $\times 10^3$ cells in 6 well dish. Starting 48 hours post-transfection, cells were cultured in
545 selection medium with 800 μg/ml of G418 (Sigma-Aldrich, catalog number A1720) for 7
546 days, with selection medium being changed every other day. Cells were recovered in G418-
547 free medium for 4 days, after which cells were trypsinized and diluted to 0.5 cells per 200
548 μl and seeded into 96-well plates. A week later plates were inspected for wells with single
549 colonies, and 4 days after that replica plated into 2× 96-well plates. One plate was frozen
550 down, the second one used to maintain and passage the cells. Once cells on the third plate

551 were at least ~70% confluent, DNA was extracted using QuickExtract DNA extraction
552 solution and PCR amplified using the following primers.
553 F3 primer: TGGCCCATTTATGAGAAAACTGA
554 R2 primer: GGGAACAGACTTCAATTCTCCA
555 1523 bp PCR products were further digested with EcoO109I restriction enzyme (New
556 England Biolabs, catalog number R0503S). PCR products from successfully integrated
557 clones were expected to be digested at 751 and 772 bp. PCR products for clones positive
558 for the EcoO109I digested bands were ran on agarose gel, purified using Zymoclean Gel
559 DNA recovery kit and sent to Genewiz for Sanger sequencing. Primers F2 and R2 shown
560 above were used for Sanger sequencing.
561
562 **Immunofluorescence**
563 Cells grown on glass coverslips were fixed in 4% paraformaldehyde for 10 min and then
564 permeabilized with 0.5% Triton X-100 for 10 min at room temperature. The fixed cells
565 were blocked in 5 % goat serum for 30 min, and incubated in primary antibody at 37 ^{0}C in
566 a humidified chamber for 1h. The cells were washed with PBS for 5 min three times,
567 incubated with secondary antibody for 1 h at 37 ^{0}C in humidified chamber, followed by
568 three PBS washes, 5 min each. Slides were then incubated with 130 ng/ml 4,6-diamidino-2-
569 phenylindole (DAPI) for 5 min and mounted in Vectashield mounting medium (Vector Lab,
570 H-1000)
571 Images were taken on a Zeiss Axioplan2 microscope with a 63× objective. Entire cells were
572 imaged via Z stacks taken at 200 nm step-intervals. Approximately 25 stacks were taken

573 per cell, and displayed as 2D maximum intensity projections generated using AxioVision
574 version 4.6.
575 The Xi-nucleolar association frequencies were scored in a blinded manner. Entire cells
576 were imaged via Z stacks taken at 200 nm step-intervals. Approximately 25 stacks were
577 taken per cell, and displayed as 2D maximum intensity projections generated using
578 AxioVision version 4.6. The Xi-nucleolar association frequencies on individual coverslips
579 were scored in a blinded manner. The criteria for Xi-nucleolar or lamina association was
580 that there were no pixels between the fluorescence signals from the XIST FISH probe and
581 fibrillarin immunostaining (for nucleolar association) or DAPI staining of the nuclear edge
582 (for lamina association). Densitometry of individual immunostained cells was performed in
583 Image J 10.2 (48), using the macro script of the RGB Profiles Tool for all experiments. The
584 quantifications of H3K27me3, macroH2.A and H4K20me1, Cot-1 and Pol II enrichment
585 were also performed in Image J 10.2 (48).
586
587 **Visualization of 5-ethynyl-2-deoxyuridine(EdU)-labeled nascent DNA**
588 hTERT-RPE1 cells were grown on glass coverslips in DMEM/F12 media as described above.
589 5-ethynyl-2-deoxyuridine (EdU) was added to the culture medium at concentration of 10
590 μM for 20 min. After labeling, cells were washed three times with PBS. Cells were then
591 permeablized in 0.5% Triton X-100 for 30 seconds and then fixed in 10% formaldehyde for
592 10 min. Cells were then rinsed twice with PBS and then incubated 30 min in 100 mM Tris-
593 HCl pH 8.5, 1 mM $CuSO_4$, 100 mM ascorbic acid plus 50 mM carboxyrhodamine 110-azide
594 for click-chemistry labeling. After staining, the cells on coverslips were washed three times

595 with PBS plus 0.5% Triton X-100, 5 min each. Cells were then counterstained with DAPI,
596 mounted in Vectashield and imaged by fluorescence microscopy as above.
597
598 **Immuno-RNA-FISH and RNA-FISH**
599 The plasmid pGIA which contains human XIST exons 4, 5 and 6 was a gift from Dr Judith
600 Sharp. Cot-1 probe was from Invitrogen (Sigma 11581074001). The probes were labeled
601 either with biotin-14-dCTP or digoxigenin-11-dUTP using the BioPrime DNA labeling
602 system (Invitrogen 18094-011).
603 For immunofluorescence (IF) combined with RNA-FISH, IF was performed first as above.
604 Cells were then re-fixed in 4% paraformaldehyde for 10 min at room temperature. The
605 cells were then dehydrated in 75%, 85%, 95% and 100% ethanol for 2 min each.
606
607 Approximately 150 ng of each probe was mixed with 20 μg single-stranded salmon sperm
608 DNA (Sigma-Aldrich) and 12 μg E. coli tRNA and then air-dried in a speed vacuum,
609 resuspended in 20 l 50% formamide / 50% hybridization buffer (20% Dextran Sulfate in
610 4× SSC), denatured at 80 ^{0}C for 10 min and pre-annealed at 37 ^{0}C for 30 min prior to
611 hybridization. Hybridizations were performed overnight in a humidified chamber at 37^{0}C.
612 The next day, cells were washed for 20 min in 50% formamide in 2× SSC at 37°C and then
613 for 20 min in 2× SSC at 37°C and 20 min in 1× SSC at 37°C. The hybridized probes were
614 detected by incubation with either Alexa fluor-488 conjugated to streptavidin (Invitrogen
615 S-32354) or Dylight 594 labeled anti-Digoxigenin/Digoxin (Vector Labs, DI-7594) at 1:500
616 dilutions for 60 min in a 37^{0}C humid chamber. After incubation, slides were washed twice

617 in 50% formamide, 2× SSC for 5 min and once in 1× SSC for 5 min in a 37^{0}C humid chamber

618 before DAPI staining as above.

619

620 **RNAi experiments**

621 The siRNA targeting human Ki-67 is from the collection of Silencer Select Predesigned

622 siRNAs (Thermo Fisher Scientific), and targets nucleotides 559-577 of the cDNA

623 (NM_002417.4).

624 Its sequence is as follows:

625 sense CGUCGUGUCUCAAGAUCUAtt,

626 antisense UAGAUCUUGAGACACGACGtg

627 TP53 (NM_00546.5)

628 Forward primer for hTP53: GAAAUUUGCGUGUGGAGUAtt

629 Reverse primer for hTP53:UACUCCACACGCAAAUUUCct

630 p21(NM_078467.2)

631 Forward primer for hp21: CAAGGAGUCAGACAUUUUAtt

632 Reverse primer for hp21: UAAAAUGUCUGACUCCUUGtt

633

634 esiRNA targeting human Ki-67 was generated by in vitro RNaseIII cleavage of T7 RNA

635 polymerase-synthesized transcripts, as previously described (21,67), and targets internal

636 repeat regions at nucleotides 3611-4047, 3979-4357, 4705-5098 and 6913-7347 of the

637 cDNA (NM_002417.4).

638 Forward primer for hKi-67

639 gcgtaatacgactcactataggGTGCTGCCGGTTAAGTTCTCT

640 Reverse primer for hKi-67

641 gcgtaatacgactcactataggGCTCCAACAAGCACAAAGCAA

642 Forward primer for luciferase

643 gcgtaatacgactcactataggAACAATTGCTTTTACAGATGC

644 Reverse primer for luciferase

645 gcgtaatacgactcactataggAGGCAGACCAGTAGATCC

646 Cells were transfected with Lipofectamine RNAi MAX (Invitrogen Catalog number

647 13778100) following manufacturer's instructions.

648 For esiRNA transfection, 500ng of esiRNA targeting either luciferase control or Ki-67 was

649 transfected into 40×10^3 cells in a 6-well dish.

650 For siRNA transfection, 40 nM of either scramble or siKi-67 was transfected into 40×10^3

651 cells in a 6-well dish.

652 The cells were harvested 72 hrs after transfection for immunoblotting, RT-qPCR, RNA-seq,

653 FACS or FISH analysis.

654

655 **Flow cytometry**

656 BrdU incorporation was analyzed based on published prototcols (68). Cells were pulsed

657 labeled with 50 μM bromodexoyuridine (BrdU) for the indicated time periods. Cells were

658 then washed twice with PBS and fixed in 70% ethanol at 4^{0}C for 1 hour. Post-fixed cells

659 were denatured in 2N HCl/0.5% Triton-X for 30 minutes. After denaturation, cells were

660 washed once in 0.1 M sodium tetraborate for 2 minutes and once in PBS/1% BSA. After

661 that, cells were resuspended in 1 μg/ml anti-BrdU antibody/PBS/1% BSA for 1 hr, followed

662 by three washes with 0.5% Tween 20/1% BSA/PBS. The cells were incubated with 0.5

663 μg/ml secondary antibody/PBS/1% BSA for 30 minutes and counterstained with 50 μg/ml
664 propidium iodide / PBS and analyzed on a LSR II (BD Biosciences). The data was analyzed
665 with FlowJo v9.9.4 software (TreeStar, Ashland, OR).
666
667 **RNA isolation and real time quantitative PCR**
668 Total RNA from cells 72 hours post-transfection was isolated using Trizol (Invitrogen
669 15596026) following manufacturer's instructions and purified using the RNeasy kit
670 (Qiagen 74104).
671 One microgram of RNA was subjected to reverse transcription with SuperScript II Reverse
672 Transcriptase (Invitrogen 18064014). qPCR reactions were performed on an Applied
673 Biosystem StepOnePlus machine (Life Technologies) using FAST SYBR mix (KAPA
674 Biosystem). The program used is as follows: hold 98°C for 30 s, followed by 40 cycles of
675 95°C for 10 s and 60°C for 30 s. All the signals were normalized with beta-actin as indicated
676 in the figure legends and the $2^{-\Delta\Delta Ct}$ method was used for quantification (Life technologies).
677 Primer sequences are designed by Primer3Plus software (69). All oligonucleotides for
678 qPCR are listed in Supplemental Table 5.
679
680 **RNAseq: sample preparation and analysis**
681 RNA was isolated as described above. Libraries from two replicates for each condition were
682 constructed in a strand-specific manner via the dUTP method by BGI and sequenced using
683 Illumina-HiSeq 2000/2500 platform (BGI) as single-end 50-base reads. 29M and 31M
684 mapped reads were obtained from two si-scramble-treated controls, 28M and 29M were
685 obtained from two siKi-67 knockdown replicates.

686 Reads were aligned to the human reference genome (hg19) using Tophat 2.0.14 (70,71).
687 Differential expression analysis was determined by Cufflinks 2.2.1 (72). In addition, the
688 Reactome analyses were performed using Bioconductor package ChIPpeakAnno (version
689 3.2.0)(73,74). Genes that showed differential expression with BH-adjusted q value < 0.05
690 (75) between control and Ki-67 depletion samples were selected for the Reactome analysis.
691
692 For the SNP analysis, the genotype (SNPs) information of the RPE cell line (76) from GEO
693 sample GSM1848919.
694 (https://www.ncbi.nlm.nih.gov/geo/query/acc.cgi?acc=GSM1848919) was annotated
695 based on R bioconductor package "SNPlocs.Hsapiens.dbSNP144.GRCh38".
696 *SNPlocs.Hsapiens.dbSNP144.GRCh38: SNP locations for Homo sapiens (dbSNP Build 144)*. R
697 package version 0.99.20.) The SNP locations were further annotated by ChipPeakAnno
698 package (73).
699
700 **Accession Numbers**
701 The data discussed in this publication have been deposited in NCBI's Sequence Read
702 Archive (SRA, http://www.ncbi.nlm.nih.gov/sra/) and are accessible through SRA Series
703 accession number SRR4252548.
704
705 Acknowledgments
706 We would like to thank Michael Brodsky for the generous use of the AxioPlan microscope.
707 This work was supported by NIH grants R01 GM55712 and U01 DA040588 to PDK.
708

709 References

710 1. **Gerdes J**, **Schwab U**, **Lemke H**, **Stein H**. 1983. Production of a mouse monoclonal
711 antibody reactive with a human nuclear antigen associated with cell proliferation. Int
712 J Cancer **31**:13–20.

713 2. **Gerdes J**, **Lemke H**, **Baisch H**, **Wacker HH**, **Schwab U**, **Stein H**. 1984. Cell cycle
714 analysis of a cell proliferation-associated human nuclear antigen defined by the
715 monoclonal antibody Ki-67. J Immunol **133**:1710–1715.

716 3. **Gerdes J**, **Stein H**, **Pileri S**, **Mt R**, **Gobbi M**, **Ralfkiaer E**, **Km N**, **Pallesen G**, **Bartels**
717 **H**, **Palestro G**. 1987. Prognostic relevance of tumour-cell growth fraction in
718 malignant non- Hodgkin's lymphomas. Lancet **2**:448–449.

719 4. **Dowsett M**, **Nielsen TO**, **A'Hern R**, **Bartlett J**, **Coombes RC**, **Cuzick J**, **Ellis M**, **Henry**
720 **NL**, **Hugh JC**, **Lively T**, **McShane L**, **Paik S**, **Penault-Llorca F**, **Prudkin L**, **Regan M**,
721 **Salter J**, **Sotiriou C**, **Smith IE**, **Viale G**, **Zujewski JA**, **Hayes DF**. 2011. Assessment of
722 Ki67 in Breast Cancer: Recommendations from the international Ki67 in breast
723 cancer working Group. J Natl Cancer Inst **103**:1656–1664.

724 5. **Verheijen R**, **Kuijpers HJ**, **Schlingemann RO**, **Boehmer AL**, **van Driel R**,
725 **Brakenhoff GJ**, **Ramaekers FC**. 1989. Ki-67 detects a nuclear matrix-associated
726 proliferation-related antigen. I. Intracellular localization during interphase. J Cell Sci
727 **92 (Pt 1)**:123–30.

728 6. **Kill IR**. 1996. Localisation of the Ki-67 antigen within the nucleolus. Evidence for a
729 fibrillarin-deficient region of the dense fibrillar component. J Cell Sci **109 (Pt**
730 **6)**:1253–1263.

731 7. **Cheutin T**, **O'Donohue M-F**, **Beorchia A**, **Klein C**, **Kaplan H**, **Ploton D**. 2003. Three-

732 dimensional organization of pKi-67: a comparative fluorescence and electron
733 tomography study using FluoroNanogold. J Histochem Cytochem **51**:1411–1423.
734 8. **Verheijen R**, **Kuijpers HJ**, **van Driel R**, **Beck JL**, **van Dierendonck JH**, **Brakenhoff**
735 **GJ**, **Ramaekers FC**. 1989. Ki-67 detects a nuclear matrix-associated proliferation-
736 related antigen. II. Localization in mitotic cells and association with chromosomes. J
737 Cell Sci **92 (Pt 4)**:531–540.
738 9. **Saiwaki T**, **Kotera I**, **Sasaki M**, **Takagi M**, **Yoneda Y**. 2005. In vivo dynamics and
739 kinetics of pKi-67: Transition from a mobile to an immobile form at the onset of
740 anaphase. Exp Cell Res **308**:123–134.
741 10. **Takagi M**, **Nishiyama Y**, **Taguchi A**, **Imamoto N**. 2014. Ki67 antigen contributes to
742 the timely accumulation of protein phosphatase 1γ on anaphase chromosomes. J Biol
743 Chem **289**:22877–22887.
744 11. **Booth DG**, **Takagi M**, **Sanchez-Pulido L**, **Petfalski E**, **Vargiu G**, **Samejima K**,
745 **Imamoto N**, **Ponting CP**, **Tollervey D**, **Earnshaw WC**, **Vagnarelli P**. 2014. Ki-67 is a
746 PP1-interacting protein that organises the mitotic chromosome periphery. Elife
747 **3:e01641**.
748 12. **Sobecki M**, **Mrouj K**, **Camasses A**, **Parisis N**, **Nicolas E**, **Lleres D**, **Gerbe F**, **Prieto S**,
749 **Krasinska L**, **David A**, **Eguren M**, **Birling MC**, **Urbach S**, **Hem S**, **Dejardin J**,
750 **Malumbres M**, **Jay P**, **Dulic V**, **Lafontaine DLJ**, **Feil R**, **Fisher D**. 2016. The cell
751 proliferation antigen Ki-67 organises heterochromatin. Elife **5:e13722**.
752 13. **Van Hooser AA**, **Yuh P**, **Heald R**. 2005. The perichromosomal layer. Chromosoma
753 **114**:377–388.
754 14. **Booth DG**, **Beckett AJ**, **Molina O**, **Samejima I**, **Masumoto H**, **Kouprina N**, **Larionov**

755 **V**, **Prior IA**, **Earnshaw WC**. 2016. 3D-CLEM Reveals that a Major Portion of Mitotic
756 Chromosomes Is Not Chromatin. Mol Cell **64**:790–802.
757 15. **Cuylen S**, **Blaukopf C**, **Politi AZ**, **Müller-Reichert T**, **Neumann B**, **Poser I**,
758 **Ellenberg J**, **Hyman AA**, **Gerlich DW**. 2016. Ki-67 acts as a biological surfactant to
759 disperse mitotic chromosomes. Nature **535**:308–312.
760 16. **Kumar GS**, **Gokhan E**, **De Munter S**, **Bollen M**, **Vagnarelli P**, **Peti W**, **Page R**. 2016.
761 The Ki-67 and RepoMan mitotic phosphatases assemble via an identical, yet novel
762 mechanism. Elife **5:e16539**.
763 17. **Schluter C**, **Duchrow M**, **Wohlenberg C**, **Becker MHG**, **Key G**, **Flad - HD**, **Gerdes J**.
764 1993. The cell proliferation-associated antigen of antibody Ki-67: A very large,
765 ubiquitous nuclear protein with numerous repeated elements, representing a new
766 kind of cell cycle-maintaining proteins. J Cell Biol **123**:513–522.
767 18. **Kausch I**, **Lingnau A**, **Endl E**, **Sellmann K**, **Deinert I**, **Ratliff TL**, **Jocham D**, **Sczakiel**
768 **G**, **Gerdes J**, **Böhle A**. 2003. Antisense treatment against Ki-67 mRNA inhibits
769 proliferation and tumor growth in vitro and in vivo. Int J Cancer **105**:710–716.
770 19. **Zheng J**, **Ma T**, **Cao J**, **Sun X**, **Chen J**, **Li W**, **Wen R**, **Sun Y**, **Pei D**. 2006. Knockdown of
771 Ki-67 by small interfering RNA leads to inhibition of proliferation and induction of
772 apoptosis in human renal carcinoma cells. Life Sci **78**:724–9.
773 20. **Cidado J**, **Wong HY**, **Rosen DM**, **Cimino-mathews A**, **Garay JP**, **Fessler AG**,
774 **Rasheed ZA**, **Hicks J**, **Cochran RL**, **Croessmann S**, **Zabransky DJ**, **Mohseni M**,
775 **Beaver JA**, **Chu D**, **Cravero K**, **Christenson ES**, **Medford A**, **Mattox A**, **De Marzo AM**,
776 **Argani P**, **Chawla A**, **Hurley PJ**, **Lauring J**, **Park BH**. 2016. Ki-67 is required for
777 maintenance of cancer stem cells but not cell proliferation. Oncotarget **7**:6281–6293.

778 21. **Smith CL**, **Matheson TD**, **Trombly DJ**, **Sun X**, **Campeau E**, **Han X**, **Yates JR**,
779 **Kaufman PD**. 2014. A separable domain of the p150 subunit of human chromatin
780 assembly factor-1 promotes protein and chromosome associations with nucleoli. Mol
781 Biol Cell **25**:2866–81.
782 22. **Matheson TD**, **Kaufman PD**. 2017. The p150N domain of Chromatin Assembly
783 Factor-1 regulates Ki-67 accumulation on the mitotic perichromosomal layer. Mol
784 Biol Cell **28 (1)**:21–29.
785 23. **Bodnar AG**, **Ouellette M**, **Frolkis M**, **Holt SE**, **Chiu CP**, **Morin GB**, **Harley CB**, **Shay**
786 **JW**, **Lichtsteiner S**, **Wright WE**. 1998. Extension of life-span by introduction of
787 telomerase into normal human cells. Science **279**:349–52.
788 24. **Zhang LF**, **Huynh KD**, **Lee JT**. 2007. Perinucleolar Targeting of the Inactive X during
789 S Phase: Evidence for a Role in the Maintenance of Silencing. Cell **129**:693–706.
790 25. **Dimitrova DS**, **Berezney R**. 2002. The spatio-temporal organization of DNA
791 replication sites is identical in primary, immortalized and transformed mammalian
792 cells. J Cell Sci **115**:4037–4051.
793 26. **Fischer M**, **Grossmann P**, **Padi M**, **DeCaprio JA**. 2016. Integration of TP53, DREAM,
794 MMB-FOXM1 and RB-E2F target gene analyses identifies cell cycle gene regulatory
795 networks. Nucleic Acids Res **44**:6070–6086.
796 27. **Sadasivam S**, **DeCaprio JA**. 2013. The DREAM complex: master coordinator of cell
797 cycle-dependent gene expression. Nat Rev Cancer **13**:585–595.
798 28. **Bertoli C**, **Skotheim JM**, **de Bruin RAM**. 2013. Control of cell cycle transcription
799 during G1 and S phases. Nat Rev Mol Cell Biol **14**:518–28.
800 29. **Manning AL**, **Yazinski SA**, **Nicolay B**, **Bryll A**, **Zou L**, **Dyson NJ**. 2014. Suppression of

801 genome instability in prb-deficient cells by enhancement of chromosome cohesion.
802 Mol Cell **53**:993–1004.
803 30. **Litovchick L**, **Sadasivam S**, **Florens L**, **Zhu X**, **Swanson SK**, **Velmurugan S**, **Chen R**,
804 **Washburn MP**, **Liu XS**, **DeCaprio JA**. 2007. Evolutionarily Conserved Multisubunit
805 RBL2/p130 and E2F4 Protein Complex Represses Human Cell Cycle-Dependent
806 Genes in Quiescence. Mol Cell **26**:539–551.
807 31. **Schmit F**, **Korenjak M**, **Mannefeld M**, **Schmitt K**, **Franke C**, **Von Eyss B**, **Gagrica S**,
808 **Hänel F**, **Brehm A**, **Gaubatz S**. 2007. LINC, a human complex that is related to pRB-
809 containing complexes in invertebrates regulates the expression of G2/M genes. Cell
810 Cycle **6**:1903–1913.
811 32. **Xiong Y**, **Hannon GJ**, **Zhang H**, **Casso D**, **Kobayashi R**, **Beach D**. 1993. p21 is a
812 universal inhibitor of cyclin kinases. Nature **363**:210–211.
813 33. **Gartel AL**, **Radhakrishnan SK**. 2005. Lost in transcription: p21 repression,
814 mechanisms, and consequences. Cancer Res **65**:3980–3985.
815 34. **Labaer J**, **Garrett MD**, **Stevenson LF**, **Slingerland JM**, **Sandhu C**, **Chou HS**, **Fattaey**
816 **A**, **Harlow E**. 1997. New functional activities for the p21 family of CDK inhibitors.
817 Genes Dev **11**:847–862.
818 35. **Waga S**, **Stillman B**. 1998. Cyclin-dependent kinase inhibitor p21 modulates the
819 DNA primer-template recognition complex. Mol Cell Biol **18**:4177–87.
820 36. **El-Deiry WS**, **Tokino T**, **Velculescu VE**, **Levy DB**, **Parsons R**, **Trent JM**, **Lin D**,
821 **Mercer WE**, **Kinzler KW**, **Vogelstein B**. 1993. WAF1, a potential mediator of p53
822 tumor suppression. Cell **75**:817–825.
823 37. **Deng C**, **Zhang P**, **Harper JW**, **Elledge SJ**, **Leder P**. 1995. Mice lacking

824 p21CIP1/WAF1 undergo normal development, but are defective in G1 checkpoint
825 control. Cell **82**:675–684.
826 38. **Junk DJ**, **Vrba L**, **Watts GS**, **Oshiro MM**, **Martinez JD**, **Futscher BW**. 2008. Different
827 mutant/wild-type p53 combinations cause a spectrum of increased invasive
828 potential in nonmalignant immortalized human mammary epithelial cells. Neoplasia
829 **10**:450–61.
830 39. **Petersen G.B, Therelsen A. J**. 1962. Number of nucleoli in female and male human
831 cells in tissue culture. Exp Cell Res **28**:590–2.
832 40. **Barr ML**, **Bertram EG**. 1949. A morphological distinction between neurones of the
833 male and female, and the behaviour of the nucleolar satellite during accelerated
834 nucleoprotein synthesis. Nature **163**:676.
835 41. **Bourgeois CA**, **Laquerriere F**, **Hemon D**, **Hubert J**, **Bouteille M**. 1985. New data on
836 the in situ position of the inactive X chromosome in the interphase nucleus of human
837 fibroblasts. Hum Genet **69**:122–129.
838 42. **Lucchesi JC**, **Kelly WG**, **Panning B**. 2005. Chromatin Remodeling in Dosage
839 Compensation. Annu Rev Genet **39**:615–651.
840 43. **Kohlmaier A**, **Savarese F**, **Lachner M**, **Martens J**, **Jenuwein T**, **Wutz A**. 2004. A
841 chromosomal memory triggered by Xist regulates histone methylation in X
842 inactivation. PLoS Biol **2**:E171.
843 44. **Cao R**, **Wang L**, **Wang H**, **Xia L**, **Erdjument-Bromage H**, **Tempst P**, **Jones RS**, **Zhang**
844 **Y**. 2002. Role of histone H3 lysine 27 methylation in Polycomb-group silencing.
845 Science **298**:1039–1043.
846 45. **Di Croce L**, **Helin K**. 2013. Transcriptional regulation by Polycomb group proteins.

847 natrure strucutral Mol Biol **20**:1147–55.

848 46. **Simon JA**, **Kingston RE**. 2013. Occupying chromatin: Polycomb mechanisms for
849 getting to genomic targets, stopping transcriptional traffic, and staying put. Mol Cell
850 **49**:808–24.

851 47. **Beck DB**, **Burton A**, **Oda H**, **Ziegler-Birling C**, **Torres-Padilla ME**, **Reinberg D**.
852 2012. The role of PR-Set7 in replication licensing depends on Suv4-20h. Genes Dev
853 **26**:2580–2589.

854 48. **Chaligné R**, **Popova T**, **Mendoza-Parra MA**, **Saleem MAM**, **Gentien D**, **Ban K**,
855 **Piolot T**, **Leroy O**, **Mariani O**, **Gronemeyer H**, **Vincent-Salomon A**, **Stern MH**,
856 **Heard E**. 2015. The inactive X chromosome is epigenetically unstable and
857 transcriptionally labile in breast cancer. Genome Res **25**:488–503.

858 49. **Politz JCR**, **Scalzo D**, **Groudine M**. 2016. The redundancy of the mammalian
859 heterochromatic compartment. Curr Opin Genet Dev **37**:1–8.

860 50. **Kind J**, **Pagie L**, **Ortabozkoyun H**, **Boyle S**, **De Vries SS**, **Janssen H**, **Amendola M**,
861 **Nolen LD**, **Bickmore WA**, **Van Steensel B**. 2013. Single-cell dynamics of genome-
862 nuclear lamina interactions. Cell **153**:178–192.

863 51. **Koningsbruggen S van**, **Gierlinski M**, **Schofield P**, **Martin D**, **Barton GJ**, **Ariyurek**
864 **Y**, **Dunnen JT den**, **Lamond AI**. 2010. High-Resolution Whole-Genome Sequencing
865 Reveals That Specific Chromatin Domains from Most Human Chromosomes
866 Associate with Nucleoli. Mol Biol Cell **21**:3735–3748.

867 52. **Ragoczy T**, **Telling A**, **Scalzo D**, **Kooperberg C**, **Groudine M**. 2014. Functional
868 redundancy in the nuclear compartmentalization of the late-replicating genome.
869 Nucleus **5**:626–35.

870 53. **Ma H**, **Naseri A**, **Reyes-Gutierrez P**, **Wolfe SA**, **Zhang S**, **Pederson T**. 2015.
871 Multicolor CRISPR lableing of chromosomal loci in human cells. Proc Natl Acad Sci U
872 S A **112**:3002–7.
873 54. **Benson EK**, **Mungamuri SK**, **Attie O**, **Kracikova M**, **Sachidanandam R**, **Manfredi JJ**,
874 **Aaronson S a**. 2014. p53-dependent gene repression through p21 is mediated by
875 recruitment of E2F4 repression complexes. Oncogene **33**:3959–69.
876 55. **Sobecki M**, **Mrouj K**, **Colinge J**, **Gerbe F**, **Jay P**, **Krasinska L**, **Dulic V**, **Fisher D**.
877 2017. Cell cycle regulation accounts for variability in Ki-67 expression levels. Cancer
878 Res canres.0707.2016.
879 56. **Brugarolas J**, **Moberg K**, **Boyd S**, **Taya Y**, **Jacks T**, **Lees JA**. 1999. Inhibition of cyclin-
880 dependent kinase 2 by p21 is necessary for retinoblastoma protein-mediated G1
881 arrest after gamma-irradiation. Proc Natl Acad Sci U S A **96**:1002–1007.
882 57. **Chubb JR**, **Boyle S**, **Perry P**, **Bickmore WA**. 2002. Chromatin motion is constrained
883 by association with nuclear compartments in human cells. Curr Biol **12**:439–445.
884 58. **Dillinger S**, **Straub T**, **Nemeth A**. 2016. Nucleolus association of chromosomal
885 domains is largely maintained in cellular senescence despite massive nuclear
886 reorganisation. BioRxiv DOI**:** http://dx.doi.org/10.1101/054908
887 59. **Németh A**, **Conesa A**, **Santoyo-Lopez J**, **Medina I**, **Montaner D**, **Péterfia B**, **Solovei**
888 **I**, **Cremer T**, **Dopazo J**, **Längst G**. 2010. Initial genomics of the human nucleolus.
889 PLoS Genet **6**:e1000889.
890 60. **Yang F**, **Deng X**, **Ma W**, **Berletch JB**, **Rabaia N**, **Wei G**, **Moore JM**, **Filippova GN**, **Xu J**,
891 **Liu Y**, **Noble WS**, **Shendure J**, **Disteche CM**. 2015. The lncRNA Firre anchors the
892 inactive X chromosome to the nucleolus by binding CTCF and maintains H3K27me3

893 methylation. Genome Biol **16:52**.

894 61. **Csankovszki G**, **Nagy A**, **Jaenisch R**. 2001. Synergism of Xist RNA, DNA methylation,
895 and histone hypoacetylation in maintaining X chromosome inactivation. J Cell Biol
896 **153**:773–783.

897 62. **Chun-Kan Chen**, **Mario Blanco**, **Constanza Jackson**, **Erik Aznauryan**, **Noah**
898 **Ollikainen**, **Christine Surka**, **Amy Chow**, **Patrick McDonel**, **Andrea Cerase**,
899 **Mitchell Guttman**. 2016. Xist recruits the X chromosome to the nuclear lamina to
900 enable chromosome-wide silencing. Science **354** : 468-472.

901 63. **Benanti JA**, **Galloway DA**. 2004. Normal human fibroblasts are resistant to RAS-
902 induced senescence. Mol Cell Biol **24**:2842–52.

903 64. **Cong L**, **Ran FA**, **Cox D**, **Lin S**, **Barretto R**, **Habib N**, **Hsu PD**, **Wu X**, **Jiang W**,
904 **Marraffini LA**, **Zhang F**. 2013. Multiplex genome engineering using CRISPR/Cas
905 systems. Science **339**: 819–23.

906 65. **Ran FA**, **Hsu PD**, **Wright J**, **Agarwala V**, **Scott DA**, **Zhang F**. 2013. Genome
907 engineering using the CRISPR-Cas9 system. Nat Protoc **8**:2281–2308.

908 66. **Brinkman EK**, **Chen T**, **Amendola M**, **Van Steensel B**. 2014. Easy quantitative
909 assessment of genome editing by sequence trace decomposition. Nucleic Acids Res
910 **42**: e168.

911 67. **Yang D**, **Buchholz F**, **Huang Z**, **Goga A**, **Chen C-Y**, **Brodsky FM**, **Bishop JM**. 2002.
912 Short RNA duplexes produced by hydrolysis with Escherichia coli RNase III mediate
913 effective RNA interference in mammalian cells. Proc Natl Acad Sci U S A **99**:9942–
914 9947.

915 68. **Zhu H**. 2012. Cell Proliferation Assay by Flow Cytometry. Bio-Protocol **Bio101**:e198.

916 69. **Untergasser A**, **Cutcutache I**, **Koressaar T**, **Ye J**, **Faircloth BC**, **Remm M**, **Rozen SG**.
917 2012. Primer3-new capabilities and interfaces. Nucleic Acids Res **40**:e115.
918 70. **Trapnell C**, **Pachter L**, **Salzberg SL**. 2009. TopHat: Discovering splice junctions with
919 RNA-Seq. Bioinformatics **25**:1105–1111.
920 71. **Kim D**, **Pertea G**, **Trapnell C**, **Pimentel H**, **Kelley R**, **Salzberg SL**. 2013. TopHat2:
921 accurate alignment of transcriptomes in the presence of insertions, deletions and
922 gene fusions. Genome Biol **14**:R36.
923 72. **Trapnell C**, **Williams B a**, **Pertea G**, **Mortazavi A**, **Kwan G**, **van Baren MJ**, **Salzberg**
924 **SL**, **Wold BJ**, **Pachter L**. 2010. Transcript assembly and abundance estimation from
925 RNA-Seq reveals thousands of new transcripts and switching among isoforms. Nat
926 Biotechnol **28**:511–515.
927 73. **Zhu** LJ, **Gazin C**, **Lawson ND**, **Pagès H**, **Lin SM**, **Lapointe DS**, **Green MR**. 2010.
928 ChIPpeakAnno: a Bioconductor package to annotate ChIP-seq and ChIP-chip data.
929 BMC Bioinformatics **11**:237.
930 74. **Zhu LJ**. 2013. Integrative Analysis of ChIP-Chip and ChIP-Seq Dataset. Methods Mol
931 Biol **1067**:105–124.
932 75. **Wright SP**. 1992. Adjustd p-values for simultaneous inference. Biometrics **48**:1005–
933 1013.
934 76. **Passerini V**, **Ozeri-Galai E**, **de Pagter MS**, **Donnelly N**, **Schmalbrock S**,
935 **Kloosterman WP**, **Kerem B**, **Storchová Z**. 2016. The presence of extra
936 chromosomes leads to genomic instability. Nat Commun **7**:10754.
937
938
939

940 Figure Legends

941

942 **Figure 1. Ki-67 depletion in hTERT-RPE1 cells reduced S-phase-related mRNA**

943 **abundance and the proportion of cells in S phase.**

944 A. Scatter plot analysis of RNA levels, comparing two replicate si-scramble RNAseq

945 analyses of hTERT-RPE1 cells. R: Pearson's correlation coefficient.

946 B. Scatter plot analysis comparing two replicate siKi-67 RNAseq analyses.

947 C. Distribution of RNA level fold changes (FC) measured by RNAseq, comparing si-

948 scramble and siKi-67-treated hTERT-RPE1 cells. The x-axis shows the mean log2 value

949 for normalized counts of abundance levels for each RNA species. The y-axis shows the

950 log2 fold change upon Ki-67 depletion. The symmetry of the plot above and below the y

951 = 0 axis indicates that similar numbers of genes are up- and down-regulated upon Ki-67

952 depletion.

953 D. Reactome evaluation of RNAseq analysis of si-Ki-67-treated cells. The PATH terms with

954 a p-value < 5e-05 are graphed.

955 E. RNA levels of DNA replication genes are coordinately down-regulated in siKi-67-treated

956 cells. RT-qPCR measurements are presented as fold change relative to the scramble

957 siRNA control after normalization. *MKI67* mRNA levels indicate effectiveness of the

958 siRNA treatment. Data are mean ± std. dev. of 3 biological replicates.

959 F. Analysis of RNA levels as in panel E, except that cells were treated with in vitro-diced

960 esiRNAs as depletion reagents.

961 G. FACS analysis of siRNA-treated cells. Cells were pulsed with BrdU for 20 min, and

962 analyzed via two-dimensional flow cytometry monitoring BrdU incorporation (y-axis)

963 and DNA content (x-axis). G1 (lower left), G2 (lower right), and S-phase populations
964 (upper box) are boxed in each sample, with percentages of the total population shown.
965 Data shown are from one representative experiment of three biological replicates
966 performed.
967 H. FACS analysis as in panel G, except that cells were treated with esiRNAs.
968 I. Quantification of percentage of cells in S-phase in siRNA-treated hTERT-RPE1
969 populations from three biological replicate BrdU-labeling experiments. p-value
970 comparing si-scramble and si-Ki-67 treatments is indicated, calculated via an unpaired,
971 two-tailed parametric t test.
972 J. Quantification of percentage of cells in G1 or G2/M phase from the same three
973 experiments analyzed in panel I.
974 K. Quantification of percentage of S-phase cells as in panel I, except that cells were treated
975 with in vitro-diced esiRNAs.
976 L. Quantification of percentage of cells in G1 or G2/M phase from the same three
977 experiments analyzed in panel K.
978 M. Immunoblot analysis of Ki-67 depletion in siRNA-treated hTERT-RPE1 cells from panel
979 D. Marker molecular weights are indicated on the left.
980 N. Immunoblot analysis of Ki-67 depletion in esiRNA-treated hTERT-RPE1 cells from
981 panel F.
982
983 **Figure 2. Validation of specificity and effectiveness of Ki-67 depletion reagents.**
984 A. CRISPR/Cas9-based strategy for generating siRNA-resistant mutations in the
985 endogenous Ki-67 gene. The si-Ki-67 target (green) and sgRNA-directed cleavage site

986 (red triangle) are indicated on the upper diagram of the endogenous locus. Altered
987 nucleotides (red) and the novel EcoO109I restriction site are shown on the lower
988 diagram of the repair template.
989 B. DNA sequence analysis of a PCR product from wild-type hTERT-RPE1 cells and si-Ki-67-
990 resistant clone #7.
991 C. EcoO109I digestion of the same PCR product sequenced in panel B.
992 D. Immunoblot analysis of clone #7 treated with the indicated reagents.
993 E. RT-qPCR analysis of clone #7.
994 F-L. Immunoblot analyses of the indicated cell lines, treated with the indicated RNA
995 depletion reagents.
996
997 **Figure 3. siRNA-mediated Ki-67 depletion affected S-phase gene expression and cell**
998 **cycle distribution in diploid human cells.**
999 WI-38 (panels A-D), IMR-90 (panels E-H), hTERT-BJ (panels I-L) cell lines and human
1000 primary fibroblasts (HFF, panels M-P) were analyzed.
1001 A, E, I, M. RT-qPCR analysis, as in Figure 1E.
1002 B, F, J, N. FACS analysis, as in Figure 1G.
1003 C, G, K, O. Quantification of percentage of S-phase cells, as in Figure 1I.
1004 D, H, L, P. Quantification of percentage of G1 and G2/M phase cells as in Figure 1J.
1005
1006 **Figure 4. esiRNA-mediated depletion of Ki-67 in diploid cells resulted in the same**
1007 **phenotypes observed with siRNA treatments.** Cells and assays were the same as in
1008 Figure 3.

1009

1010 **Figure 5. Ki-67-insensitive cells.** Ki-67 depletion did not affect S-phase gene expression
1011 and cell cycle distribution in HeLa (panels A-D), U2OS (panels E-H), and 293T (panels I-L)
1012 cell lines. Panels A, E, I: RT-qPCR analysis. Panels B, F, J: FACS analysis. Panels C, G, K:
1013 Quantification of percentage of S-phase cells. Panels D, H, L: Quantification of percentage of
1014 G1 and G2/M phase cells.

1015

1016 **Figure 6. esiRNA-mediated depletion of Ki-67 in insensitive-cells resulted in the**
1017 **same phenotypes observed with siRNA treatments.** Cells and assays were the same as
1018 in Figure 5.

1019

1020 **Figure 7. Depletion of Ki-67 delayed S-phase entry in hTERT-RPE1 cells.**

1021 A. Schematic of short-pulse assay. hTERT-RPE1 cells were released from HU arrest for the
1022 indicated time periods, pulsed for 20 min with EdU, and analyzed by click chemistry
1023 and fluorescence microscopy for EdU incorporation.

1024 B. Representative cells from the indicated time points, showing EdU staining (green) to
1025 detect the progression of S phase. Total DNA was visualized with DAPI staining (blue). S
1026 phase cells were categorized into 3 sub-stages based on the number, size, shape and
1027 distribution of fluorescent-labeled replication foci. During early S phase, small and
1028 numerous replication foci were scattered in the nuclear interior, but excluded from
1029 nucleolus, nuclear periphery and other heterochromatic regions. At mid-S phase,
1030 replication takes place at the nuclear periphery and perinucleolar regions. Late in S
1031 phase, there are several large foci throughout the nucleus (25). Scale bar: 5 μm.

1032 C. Distributions of EdU morphologies during the time course. Percentages of early S phase,
1033 middle S phase and late S phase EdU staining morphologies were counted in >300 total
1034 cells per time point.
1035 D. FACS histograms showing cell-cycle profiles of propidium-iodide stained hTERT-RPE1
1036 cells. Asy: Asynchronous cells were incubated with DMSO vehicle control. HU block:
1037 cells were incubated with hydroxyurea. Left panel: si-scramble-treated cells were
1038 incubated with or without 2mM hydroxyurea for 15 hours. Right panel: siKi-67-treated
1039 cells were incubated with or without 2mM hydroxyurea for 15 hours. Histograms were
1040 generated using FlowJo v9.9.4.
1041 E. A longer (three hour) EdU pulse prevents detection of S phase alterations in Ki-67-
1042 depleted hTERT-RPE1 cells. Asynchronous cells were treated with either si-scramble or
1043 siKi-67 for 72 hrs, incubated with 5-ethynyl-2-deoxyuridine (EdU) for the final 3 hours,
1044 and analyzed via click chemistry. The total cells assayed = 218 for si-scramble and 265
1045 for siKi-67, in three independent experiments. Scale bar, 20 μm
1046 F. Ratio of EdU-positive cells to the total cell numbers. ns: not significant (p-value = 0.77).
1047 G. Cell cycle distribution of the si-scramble and siKi-67 treated hTERT-RPE1 cells as
1048 analyzed by one-dimensional FACS profiling of propidium iodide-stained cells.
1049
1050 **Figure 8. Rb contributes to transcriptional downregulation caused by Ki67 depletion.**
1051 A. Summary of transcriptional changes of cell cycle target genes (based on Table S10 in
1052 (26)). The "Adjusted Cell Cycle Score" on the y-axis indicates values based on meta-
1053 analysis of 5 different cell cycle expression data sets, plus information regarding
1054 binding by Rb/E2F and MMB/FOXM1 transcription factors. Negative values indicate

1055 frequent detection of G1/S expression and binding by Rb/E2F, and positive values
1056 indicate frequent detection of G2/M expression and binding by MMB-FOXM1.
1057 B. p-values of transcription changes of E2F target genes (based on Table S9 in (26)), with
1058 the greater score on the x-axis representing higher frequency of detection as an E2F
1059 target. As expected from panel A, E2F targets are commonly downregulated upon Ki-67
1060 depletion.
1061 C. Immunoblot analysis hTERT-RPE1 Tet-sh-Rb cells. Cells were treated with either
1062 vehicle (Rb+) or 2 μg/ml doxycycline (Rb-) as indicated for 72 h to induce sh-Rb
1063 expression, and were also incubated in the presence of either si-scramble (Ki-67+) or
1064 siKi-67 (Ki-67-).
1065 D. RT-qPCR analysis of DNA replication genes in cells treated as in panel C. Measurements
1066 are presented as fold change relative to the scramble siRNA control without
1067 doxycycline induction. Data are mean ± std. dev. of 3 biological replicates. p-values were
1068 calculated via unpaired, two-tailed parametric t tests and corrected for multiple
1069 comparisons using the Holm-Sidak method.
1070 E. Percentage of S phase cells calculated from three BrdU labeling experiments. p-values
1071 were calculated via unpaired, two-tailed parametric t tests.
1072 F. FACS analysis of a representative BrdU labeling experiment.
1073 G. p-values of transcription changes of DREAM target genes (based on Table S7 in (26)),
1074 with the greater score on the x-axis representing more frequent detection as a DREAM
1075 target.
1076 H. Model. In "Ki-67 sensitive" cells, depletion of Ki67 leads to p21 induction. The elevated
1077 p21 levels are predicted to downregulate the Rb/E2F and DREAM target G1/S cell cycle

1078 genes and inhibit DNA synthesis by binding to PCNA. Together, these effects delay S
1079 phase entry.

1080 **Figure 9. Cell-type-specific induction of a p21-dependent checkpoint upon depletion**
1081 **of Ki-67.**

1082 A. RT-qPCR analysis demonstrates cell-type specific induction of *CDKN1A* (p21) RNA upon
1083 Ki-67 depletion. (left panel) Indicated cells were treated with either si-scramble or si-
1084 Ki-67 for 72 hrs. (right panel) Same, except cells were treated with esiRNAs.

1085 B. Cell-type specific induction of p21 protein levels upon Ki-67 depletion. hTERT-RPE1
1086 and 293T cells were treated with the indicated siRNA or in vitro-diced esiRNA depletion
1087 reagents. p21 protein levels were quantified as a ratio to β-tubulin and normalized to
1088 levels in control-treated cells. Quantification was done in Image J 10.2.

1089 C. Immunoblot analysis of hTERT-RPE1 cells depleted of the indicated proteins via siRNA
1090 treatments. Marker molecular weights are indicated on the right.

1091 D. RT-qPCR analysis of DNA replication genes in hTERT-RPE1 cells from panel C. Asterisks
1092 indicate values in the si-p21 + si-Ki-67 samples that were significantly different ($p <$
1093 0.05) from the siKi-67 samples. p-values were calculated via unpaired, two-tailed
1094 parametric t tests and corrected for multiple comparisons using the Holm-Sidak
1095 method.

1096 E. Percentage of S phase cells calculated from three BrdU labeling experiments. p-values
1097 were calculated via unpaired, two-tailed parametric t tests.

1098 F. FACS analysis of a representative BrdU labeling experiment.

1099 G. Immunoblot analysis of additional siRNA-treated cell lines testing for p21 induction.

1100 H. RT-qPCR analysis of the indicated genes in MCF7 cells. p-values calculated as in panel D
1101 were < 0.05 for all genes.
1102 I. RT-qPCR analysis of the indicated genes in MDA-MB-231 cells.
1103 J. RT-qPCR analysis of the indicated genes in HCT-116 cells.
1104
1105
1106 **Figure 10. H3K27me3 and H4K20me1 staining of the inactive X chromosome was**
1107 **altered upon Ki-67 depletion in a subset of hTERT-RPE1 cells.** Scale bars, 5 µm.
1108 A. Immuno-FISH analysis of H3K27me3 overlap with XIST in siRNA-treated hTERT-RPE1
1109 cells. Note that in the si-Ki-67-treated cell, the H3K27me3 signal overlapping XIST
1110 displayed reduced intensity and was localized away from the nuclear lamina.
1111 B. Quantitation of percentage of cells that display reduced H3K27me3 enrichment on the
1112 Xi in the panel A experiments. Enrichment was calculated as the ratio of the mean
1113 H3K27me3 signal overlapping XIST divided by the mean H3K27me3 signal from
1114 remainder of the entire nucleus. Cells with ratios less than 1.5 were defined as having
1115 reduced enrichment, as described previously (48). Percentages were calculated for the
1116 total cell populations, as well as for the nuclear lamina-associated XIST foci and the
1117 non-lamina-associated foci, as indicated. Total cells assayed = 250 for si-scramble and
1118 239 for si-Ki-67. Mean and SDs are graphed from three biological replicate experiments.
1119 p-values were determined by unpaired student's t tests.
1120 C. Analysis of H3K27me3 enrichment on Xi as in panel A, for hTERT-RPE1 cells treated
1121 with in vitro-diced esiRNAs.
1122 D. Quantitation as in panel B. Total cells assayed= 236 for esi-luciferase, 220 for esi-Ki-67.

1123 E. Immuno-FISH analysis of H4K20me1 overlap with XIST in siRNA-treated hTERT-RPE1
1124 cells. Note that the H4K20me1 signal colocalizing with XIST is reduced in the Ki-67-
1125 depleted cell.
1126 F. Quantitation of the panel E experiments, as in panel B. The total cells assayed = 204 si-
1127 scramble and 216 for si-Ki-67.
1128 G. Analysis of H4K20me1 in cells treated with esiRNAs.
1129 H. Quantitation of the panel G experiments. Total cells assayed = 164 for esi-luciferase,
1130 182 for esi-Ki-67.
1131 I. Example of H3K27me3 signal intensity quantification.
1132 J. RT-qPCR analysis of XIST RNA levels in hTERT-RPE1 cells.
1133
1134 **Figure 11. H3K27me3 and H4K20me1 staining of the inactive X chromosome was**
1135 **unaltered upon Ki-67 depletion in 293T cells.** Scale bars, 5 μm.
1136 A. Immuno-FISH analysis of H3K27me3 overlap with XIST in siRNA-treated 293T cells.
1137 Note that 293T cells have two Xi chromosomes. In these cells, the H3K27me3 foci
1138 overlapping XIST remained unchanged upon Ki67 depletion.
1139 B. Quantitation of panel A. The total alleles assayed = 136 for si-scramble and 146 for si-
1140 Ki-67.
1141 C, D. Analysis of H3K27me3 in esiRNA-treated 293T cells. Total alleles assayed = 196 for
1142 esi-luciferase, 198 for esi-Ki-67.
1143 E. Immuno-FISH analysis of H4K20me1 overlap with XIST in 293T cells. In these cells, the
1144 H4K20me1 foci overlapping XIST remained unchanged upon Ki67 depletion.

1145 F. Quantitation of panel E. The total alleles assayed = 180 for si-scramble and 162 for si-
1146 Ki-67.
1147 G, H. Analysis of H4K20me1 in esiRNA-treated cells. Total alleles assayed = 180 for esi-
1148 luciferase, 162 for esi-Ki-67.
1149
1150 **Figure 12. Analysis of Cot-1 and Pol II enrichment on Xi in siRNA-treated hTERT-**
1151 **RPE1 cells.** Scale bars, 5 μm.
1152 A-B Localization of Cot-1-hybridizing transcripts relative to XIST domains, when XIST is
1153 localized away from (A) or at (B) the nuclear lamina. A line scan (white arrow) across
1154 the XIST signal (green) was used to analyze Cot-1 hybridization levels (red);
1155 fluorescent densities across the line scan were plotted in the right-hand panels. Cot-1
1156 RNA was considered to be reduced across the XIST domain when the average Cot-1
1157 signal overlapping XIST was lower than the average Cot-1 signal across the nucleus.
1158 The average nucleus Cot-1 signal is depicted in dotted line. In the examples shown
1159 where Xi was within the cell interior (panel A), Cot-1 RNA was excluded from XIST in
1160 the si-scramble-treated cell, but not the siKi-67-treated cell. In contrast, siKi-67
1161 treatment did not affect Cot-1 enrichment on Xi in cells where Xi was at the lamina
1162 (panel B).
1163 C-D Analysis of RNA Pol II localization (red) relative to XIST (green) when XIST is localized
1164 away from (panel C) or at (panel D) the nuclear lamina. Exclusion was analyzed as in
1165 panels A-B.
1166 E. Quantitation of Cot-1 RNA overlap with XIST RNA domains. Mean (and std. dev.)
1167 percent of cells displaying Cot-1 RNA overlapping XIST foci are plotted from three

1168 biological replicate experiments. The total cells assayed = 404 for si-scramble and 465
1169 for si-Ki-67. p-values were determined by unpaired student's t tests.
1170 F. Quantitation of percentage of cells showing presence of RNA Pol II at Xist RNA domain.
1171 The total cells assayed = 362 for si-scramble and 367 for si-Ki-67.
1172 G. Immunoblot analysis of Ki67 depletion in siRNA-treated hTERT-RPE1 cells from above.
1173
1174 **Figure 13. Analysis of Cot-1 and Pol II enrichment on Xi in esiRNA-treated hTERT-**
1175 **RPE1 cells.** Analyses were performed as in Figure 12. Scale bars, 5 μm.
1176 A, B. Cot-1. Total cells assayed= 178 for esi-luciferase, 180 for esi-Ki-67.
1177 C, D. Pol II. Total cells assayed= 160 for esi-luciferase, 176 for esi-Ki-67.
1178 E. Quantitation of Cot-1 RNA overlap with XIST RNA domains from panels A-B.
1179 F. Quantitation of RNA Pol II at Xist RNA domain from panels C-D.
1180 G. Immunoblot analysis of Ki-67 depletion in esiRNA-treated hTERT-RPE1 cells from
1181 above.
1182
1183 **Figure 14. Some aspects of Xi structure and function were resistant to Ki-67**
1184 **depletion.**
1185 A. XIST cloud in hTERT-RPE1 cells has similar appearance regardless of Ki-67 depletion.
1186 Cells were treated with the indicated siRNAs for 72 hrs and analyzed by RNA-FISH to
1187 localize XIST (green) and DAPI staining (blue). Scale bar: 10 μm.
1188 B. Average RNA levels of X linked genes did not change upon Ki-67 depletion in hTERT-
1189 RPE1 cells. log2 FPKM analyses of RNA-seq data from two biological replicates for the
1190 two indicated siRNA treatments are shown.

1191 C-H. MacroH2A enrichment at the XIST domain was not altered upon Ki-67 depletion.
1192 hTERT-RPE1 cells were treated with siRNAs (C-E) or in vitro-diced esiKi-67 (F-H) for 72
1193 hrs. Panels C, F: Cells were analyzed by immuno-RNA-FISH to localize XIST (green) and
1194 macroH2A (red). Scale bar: 10 μm. Panels D, G: Quantitation of cells that displayed reduced
1195 macroH2A staining is shown. Total cells assayed= 248 for si-scramble, 291 for siKi-67, 218
1196 for esi-luciferase, 236 for esiKi-67. Panels E, H: immunoblot analyses of Ki-67 depletions.
1197
1198
1199 **Figure 15. Depletion of Ki-67 redistributed the Xi chromosome within hTERT-RPE1**
1200 **but not 293T nuclei.** Scale bars, 10 μm.
1201 A. Fluorescence microscopy images of representative hTERT-RPE1 cells treated either
1202 with scramble control or Ki-67-targeted siRNAs as indicated. Cells were analyzed by RNA-
1203 FISH to detect XIST RNA (green) marking the Xi, and by immunofluorescence with anti-
1204 fibrillarin antibodies (red) to label nucleoli. DNA was stained with DAPI (blue).
1205 B. Quantification of XIST association frequencies from panel A experiments. XIST
1206 associations with the indicated locations were counted; "total nucleolar" indicates the sum
1207 of XIST signals that are exclusively nucleolar plus those that also are on the nuclear
1208 periphery. Three biological replicate experiments were performed with mean percentage
1209 association and SDs graphed. Total cells assayed = 363 for si-scramble, 376 for siKi-67.
1210 Holm-Sidak corrected p-values comparing si-scramble and siKi-67 treatments are
1211 indicated, with p-values < 0.05 in red.
1212 C. Fluorescence microscopy images of representative hTERT-RPE1 cells treated either
1213 with luciferase- or Ki-67-targeted esiRNAs as indicated. Cells were stained as in panel A.

1214 D. Quantification of association frequencies from panel C experiments. Total cells assayed
1215 = 348 for esi-luciferase, 391 for esiKi-67.
1216 E. Fluorescence microscopy images of representative 293T cells treated either with
1217 scramble control or Ki-67-targeted siRNAs.
1218 F. Quantification of XIST association frequencies from panel E experiments. Total alleles
1219 assayed = 272 for si-scramble, 298 for siKi-67. Holm-Sidak adjusted p-values comparing
1220 association frequencies were > 0.97 for all comparisons.
1221 G. Fluorescence microscopy images of representative 293T cells as panel E, except that
1222 cells were treated with in vitro-diced esiRNAs as depletion reagents.
1223 H. Quantitation of XIST association frequencies from panel G experiments.
1224 Total alleles assayed = 250 for esi-luciferase, 270 for esiKi-67. Holm-Sidak adjusted p-
1225 values comparing association frequencies were > 0.98 for all comparisons.
1226 Panels I-L: Frequencies of Xi associations versus time. All associations were measured in
1227 HU-synchronized cells as in Fig. 7A-B, with the averages and std. dev. from 3 independent
1228 experiments. At each time point, >300 cells were counted.
1229 I. Xi-nucleolar only associations (Xi chromosomes associated with nucleoli but not lamina).
1230 J. Xi chromosomes associated with both the lamina and nucleoli simultaneously.
1231 K. Xi-lamina only associations (Xi chromosomes associated with lamina but not nucleoli).
1232 Note that Xi-nucleolar associations (panels I-J) peak and Xi-lamina only (panel K)
1233 associations reach a minimum when the majority of cells are in mid-late S phase, which is
1234 delayed in Ki67-depleted cells by 2 hr.
1235 L. Xi-total laminar associations (Xi chromosomes associated either with the lamina or with
1236 both lamina and nucleoli simultaneously).

1237 **Legends for Supplemental tables**

1238 **Supplemental Table 1. Top reactomes detected in siKi-67 RNAseq data.**

1239 Reactome analysis of transcriptional changes reveals functional grouping of pathways

1240 altered upon Ki67 depletion in hTERT-RPE1 cells. Table shows all pathways enriched with

1241 p value < 5 x 10^{-5}. Log2FC value for selected DNA replication-related genes are shown at

1242 the bottom

1243

1244 **Supplemental Table 2. Complete RNA-seq data from siRNA-treated hTERT-RPE1**

1245 **cells.**

1246 Each transcript that mapped uniquely to the genome is listed. Value 1 is the mean FPKM

1247 from two biological replicates in si-scramble-treated hTERT-RPE1 cells. Value 2 is the

1248 mean FPKM from two biological replicates in siKi-67-treated hTERT-RPE1 cells. Fold

1249 change is the ratio of value 2 over value1 in log2 range. Status, Test_stat, p_value and q_

1250 value are generated from Cufflinks 2.2.1(1). Status: "OK" indicates a successful test,

1251 "NOTEST" indicates insufficient alignments for testing. Test_stat: displays the significance

1252 of the observed change in FPKM. p_value: uncorrected p-values of the test statistic.

1253 q_value: p-value adjusted by the false discovery rate (FDR). The criteria of significance is

1254 defined as q < 0.05.

1255

1256 **Supplemental Table 3.** Comparison of our si-Ki-67 RNAseq data to meta-analyses of cell

1257 cycle regulators (2). Separate sheets for the Cell cycle, E2F, and DREAM data are included.

1258 Cell cycle: The "Adjusted Cell Cycle Score" equals the Cell cycle expression score (Negative

1259 for G1/S-expressed genes, positive for G2/M-expressed genes, Table S10 in (2)), + 1 point

1260 for regulation by G2/M regulator MMB/FOXM1, -1 point for regulation by G1/S regulators
1261 Rb/E2F. “si-Ki-67 log2FC” and “q-values” are from the RNAseq analysis of hTERT-RPE1
1262 cells (Figure 1). Genes with the same Adjusted Cell Cycle score were analyzed in the same
1263 bin. “Significant upregulation” was TRUE if the log2FC>0 AND q<0.05. “Significant
1264 downregulation” was TRUE if log2FC<0 AND q<0.05. Benjamini-adjusted p-values (3) for
1265 these enrichments were calculated and graphed in Figure 8.
1266 E2F: The Rb/E2F binding scores come from Table S9 of (2).
1267 DREAM: The DREAM binding scores come from Table S7 of (2).
1268
1269 **Supplemental Table 4. Analysis of X-linked SNPs in the RNAseq data.**
1270 The RNAseq analyses of hTERT-RPE1 cells were compared to SNPs from the genome
1271 sequence these cells (4). We also compared these data to previous analysis of escapers
1272 from Xi silencing (5, 6).
1273
1274 **Supplemental Table 5. Oligonucleotides used in this study**
1275 Table shows primers used for RT-PCR or for generating esiRNA.
1276
1277
1278
1279
1280
1281
1282

1283

1284 Referencs for Supplemental material

1285 1. **Trapnell C**, **Williams B a**, **Pertea G**, **Mortazavi A**, **Kwan G**, **van Baren MJ**, **Salzberg**
1286 **SL**, **Wold BJ**, **Pachter L**. 2010. Transcript assembly and abundance estimation from
1287 RNA-Seq reveals thousands of new transcripts and switching among isoforms. Nat
1288 Biotechnol **28**:511–515.

1289 2. **Fischer M**, **Grossmann P**, **Padi M**, **DeCaprio JA**. 2016. Integration of TP53, DREAM,
1290 MMB-FOXM1 and RB-E2F target gene analyses identifies cell cycle gene regulatory
1291 networks. Nucleic Acids Res **44**:6070–6086.

1292 3. **Wright SP**. 1992. Adjustd p-values for simultaneous inference. Biometrics **48**:1005–
1293 1013.

1294 4. **Passerini V**, **Ozeri-Galai E**, **de Pagter MS**, **Donnelly N**, **Schmalbrock S**,
1295 **Kloosterman WP**, **Kerem B**, **Storchová Z**. 2016. The presence of extra
1296 chromosomes leads to genomic instability. Nat Commun **7**:10754.

1297 5. **Carrel L**, **Willard HF**. 2005. X-inactivation profile reveals extensive variability in X-
1298 linked gene expression in females. Nature **434**:400–404.

1299 6. **Zhang Y**, **Castillo-Morales A**, **Jiang M**, **Zhu Y**, **Hu L**, **Urrutia AO**, **Kong X**, **Hurst LD**.
1300 2013. Genes that escape X-inactivation in humans have high intraspecific variability
1301 in expression, are associated with mental impairment but are not slow evolving. Mol
1302 Biol Evol **30**:2588–2601.

1303

1304

1305

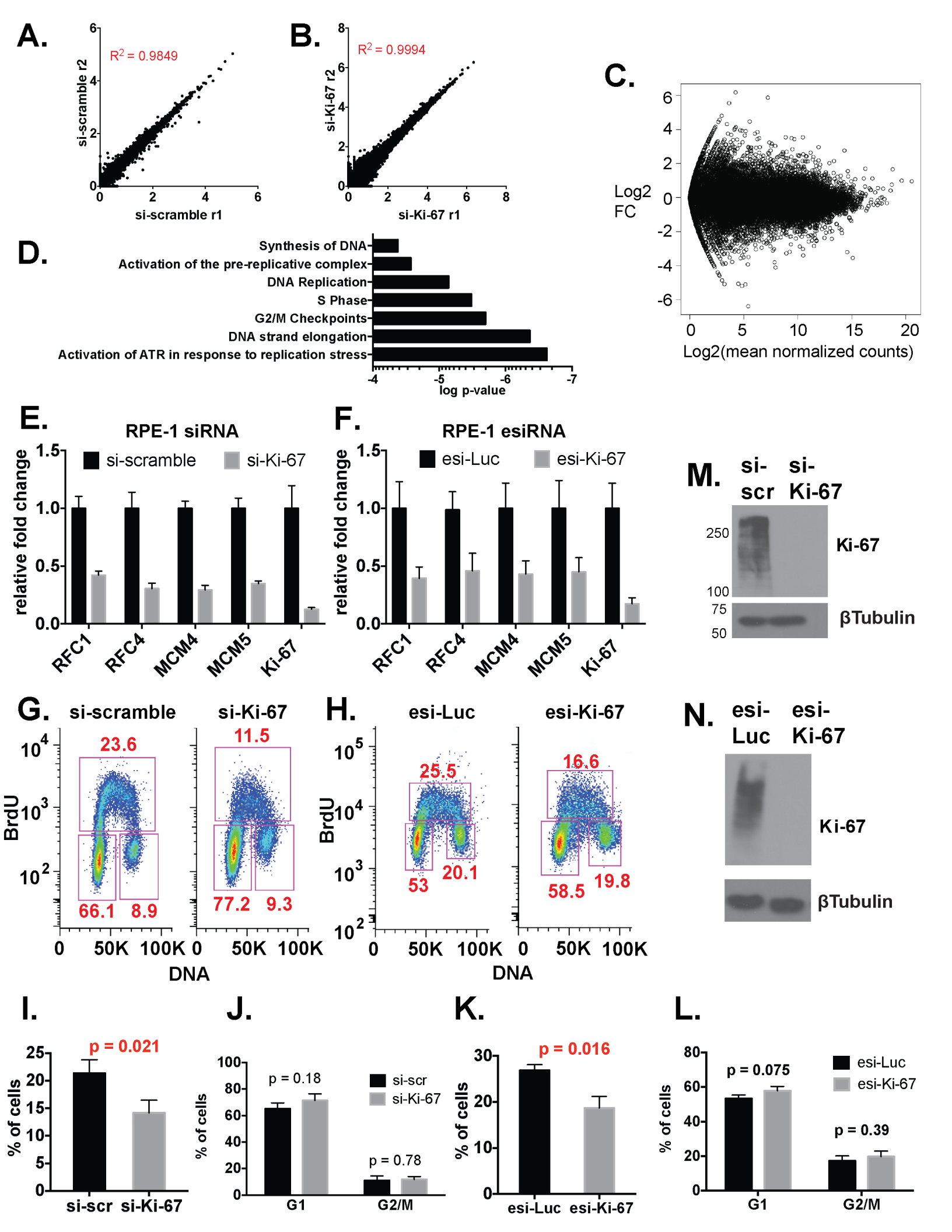
A.
R2 = 0.9849
si-scramble r2
si-scramble r1
B.
R2 = 0.9994
si-Ki-67 r2
si-Ki-67 r1
C.
Log2 FC
Log2(mean normalized counts)
D.
Synthesis of DNA
Activation of the pre-replicative complex
DNA Replication
S Phase
G2/M Checkpoints
DNA strand elongation
Activation of ATR in response to replication stress
log p-value
E.
RPE-1 siRNA
si-scramble
si-Ki-67
relative fold change
RFC1
RFC4
MCM4
MCM5
Ki-67
F.
RPE-1 esiRNA
esi-Luc
esi-Ki-67
relative fold change
RFC1
RFC4
MCM4
MCM5
Ki-67
M.
si-scr
si-Ki-67
250
100
75
50
Ki-67
βTubulin
G.
si-scramble
si-Ki-67
23.6
66.1
8.9
11.5
77.2
9.3
BrdU
DNA
H.
esi-Luc
esi-Ki-67
25.5
53
20.1
16.6
58.5
19.8
BrdU
DNA
N.
esi-Luc
esi-Ki-67
Ki-67
βTubulin
I.
p = 0.021
% of cells
si-scr
si-Ki-67
J.
p = 0.18
p = 0.78
si-scr
si-Ki-67
% of cells
G1
G2/M
K.
p = 0.016
% of cells
esi-Luc
esi-Ki-67
L.
p = 0.075
p = 0.39
esi-Luc
esi-Ki-67
% of cells
G1
G2/M

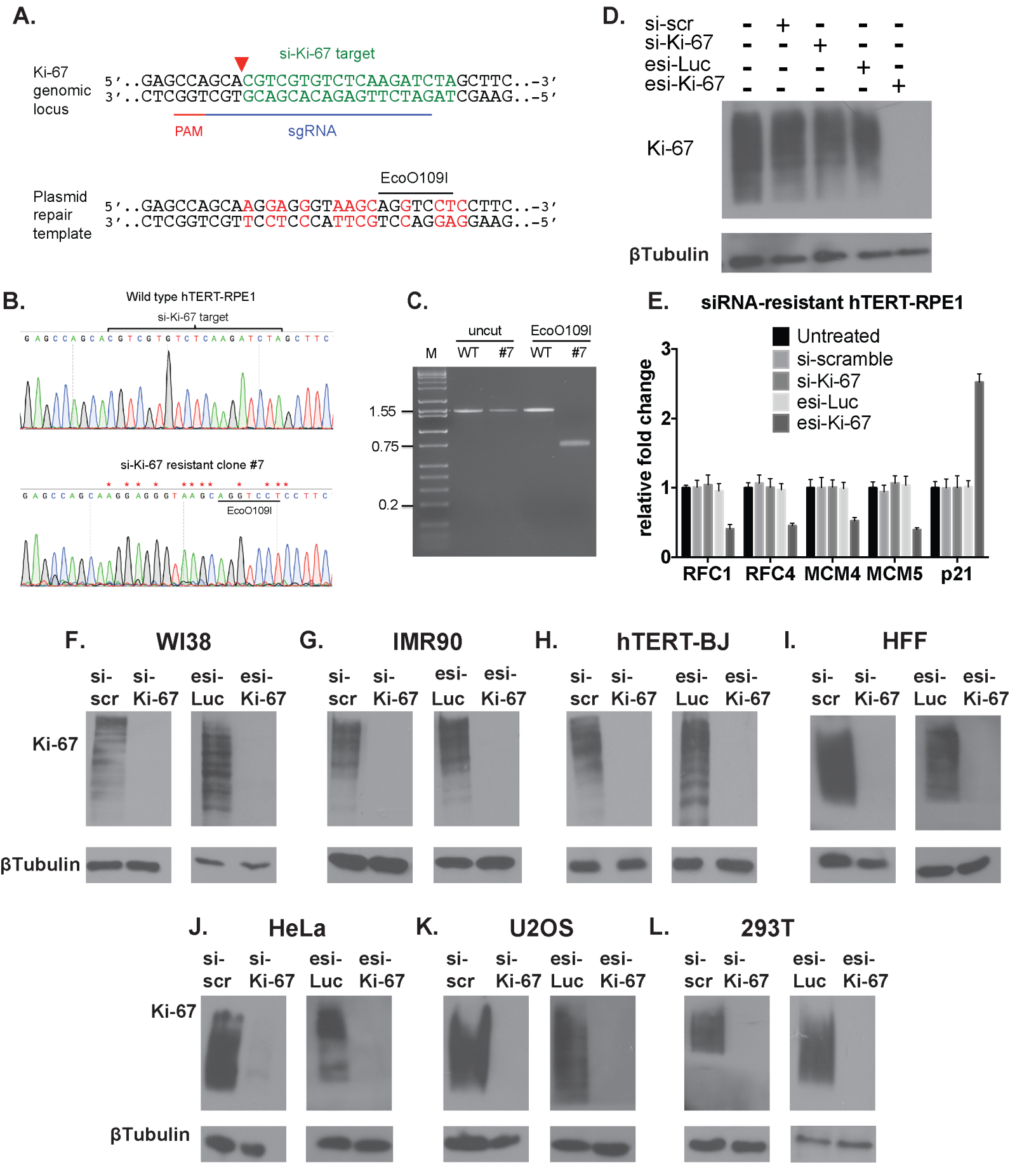
A.
si-Ki-67 target
Ki-67 genomic locus
5'..GAGCCAGCACGTCGTGTCTCAAGATCTAGCTTC..-3'
3'..CTCGGTCGTGCAGCACAGAGTTCTAGATCGAAG..-5'
PAM
sgRNA
EcoO109I
Plasmid repair template
5'..GAGCCAGCAAGGAGGGTAAGCAGGTCCTCCTTC..-3'
3'..CTCGGTCGTTCCTCCCATTCGTCCAGGAGGAAG..-5'
B.
Wild type hTERT-RPE1
si-Ki-67 target
si-Ki-67 resistant clone #7
EcoO109I
C.
uncut
EcoO109I
M
WT
#7
WT
#7
1.55
0.75
0.2
D.
si-scr
si-Ki-67
esi-Luc
esi-Ki-67
Ki-67
βTubulin
E.
siRNA-resistant hTERT-RPE1
Untreated
si-scramble
si-Ki-67
esi-Luc
esi-Ki-67
relative fold change
RFC1
RFC4
MCM4
MCM5
p21
F.
WI38
G.
IMR90
H.
hTERT-BJ
I.
HFF
si-scr
si-Ki-67
esi-Luc
esi-Ki-67
Ki-67
βTubulin
J.
HeLa
K.
U2OS
L.
293T

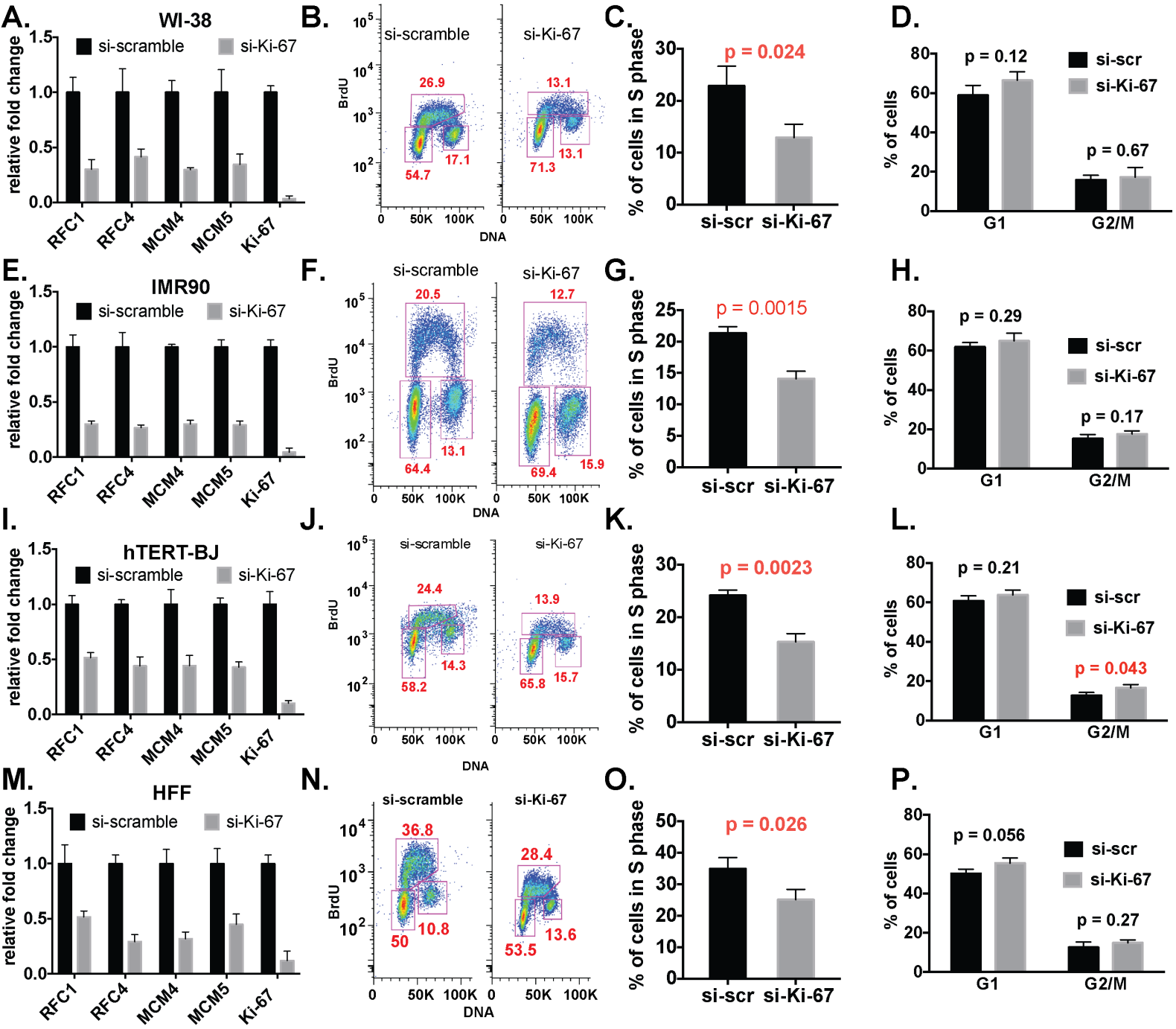
A.
WI-38
si-scramble
si-Ki-67
relative fold change
RFC1
RFC4
MCM4
MCM5
Ki-67
B.
si-scramble
si-Ki-67
BrdU
DNA
26.9
17.1
54.7
13.1
13.1
71.3
C.
% of cells in S phase
p = 0.024
si-scr
si-Ki-67
D.
% of cells
p = 0.12
p = 0.67
si-scr
si-Ki-67
G1
G2/M
E.
IMR90
F.
20.5
13.1
64.4
12.7
15.9
69.4
G.
p = 0.0015
H.
p = 0.29
p = 0.17
I.
hTERT-BJ
J.
24.4
14.3
58.2
13.9
15.7
65.8
K.
p = 0.0023
L.
p = 0.21
p = 0.043
M.
HFF
N.
36.8
10.8
50
28.4
13.6
53.5
O.
p = 0.026
P.
p = 0.056
p = 0.27

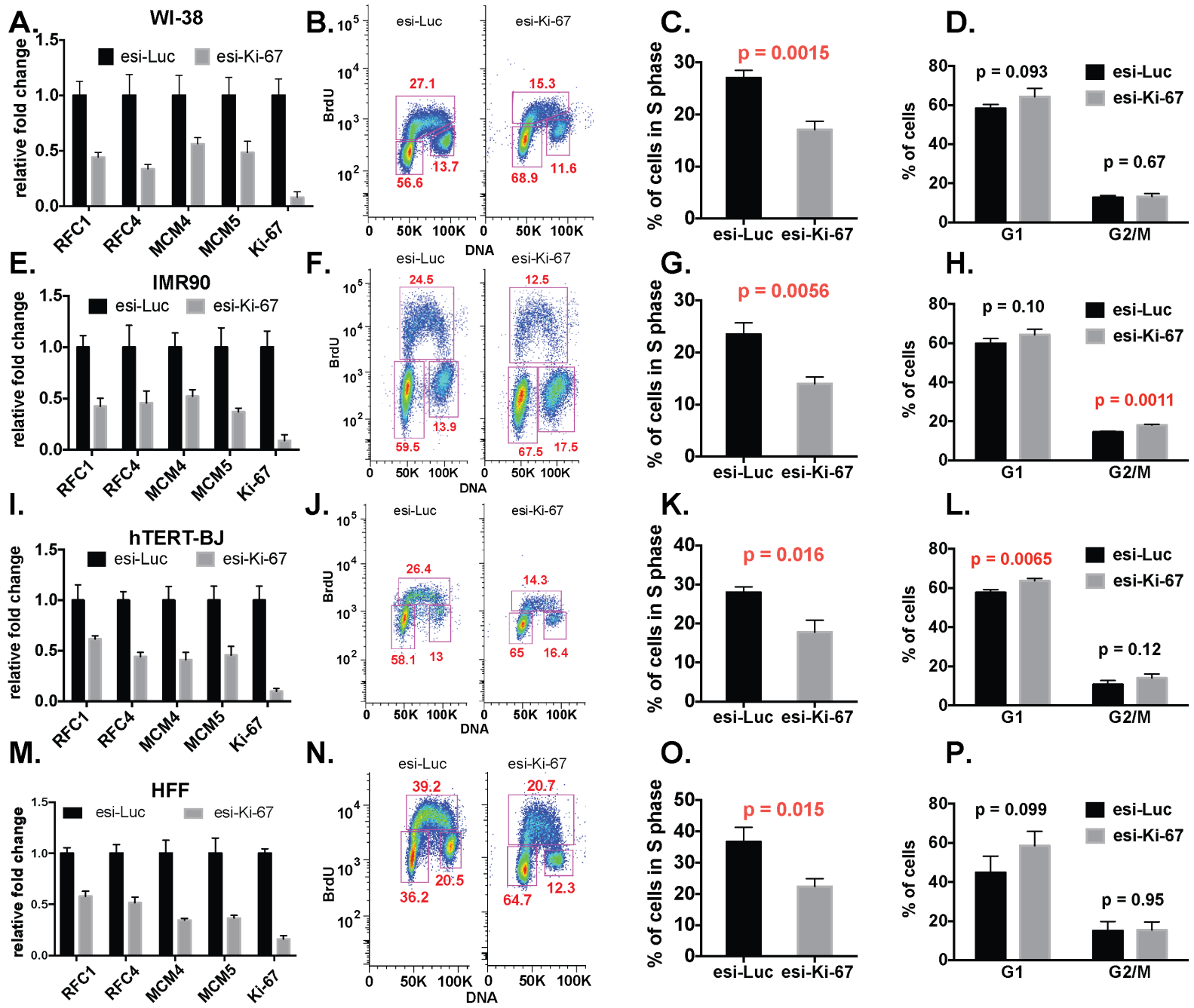
A.
WI-38
esi-Luc
esi-Ki-67
relative fold change
RFC1
RFC4
MCM4
MCM5
Ki-67
B.
esi-Luc
esi-Ki-67
BrdU
DNA
27.1
13.7
56.6
15.3
11.6
68.9
C.
p = 0.0015
% of cells in S phase
esi-Luc
esi-Ki-67
D.
p = 0.093
p = 0.67
% of cells
G1
G2/M
E.
IMR90
F.
24.5
13.9
59.5
12.5
17.5
67.5
G.
p = 0.0056
H.
p = 0.10
p = 0.0011
I.
hTERT-BJ
J.
26.4
58.1
13
14.3
65
16.4
K.
p = 0.016
L.
p = 0.0065
p = 0.12
M.
HFF
N.
39.2
36.2
20.5
20.7
64.7
12.3
O.
p = 0.015
P.
p = 0.099
p = 0.95

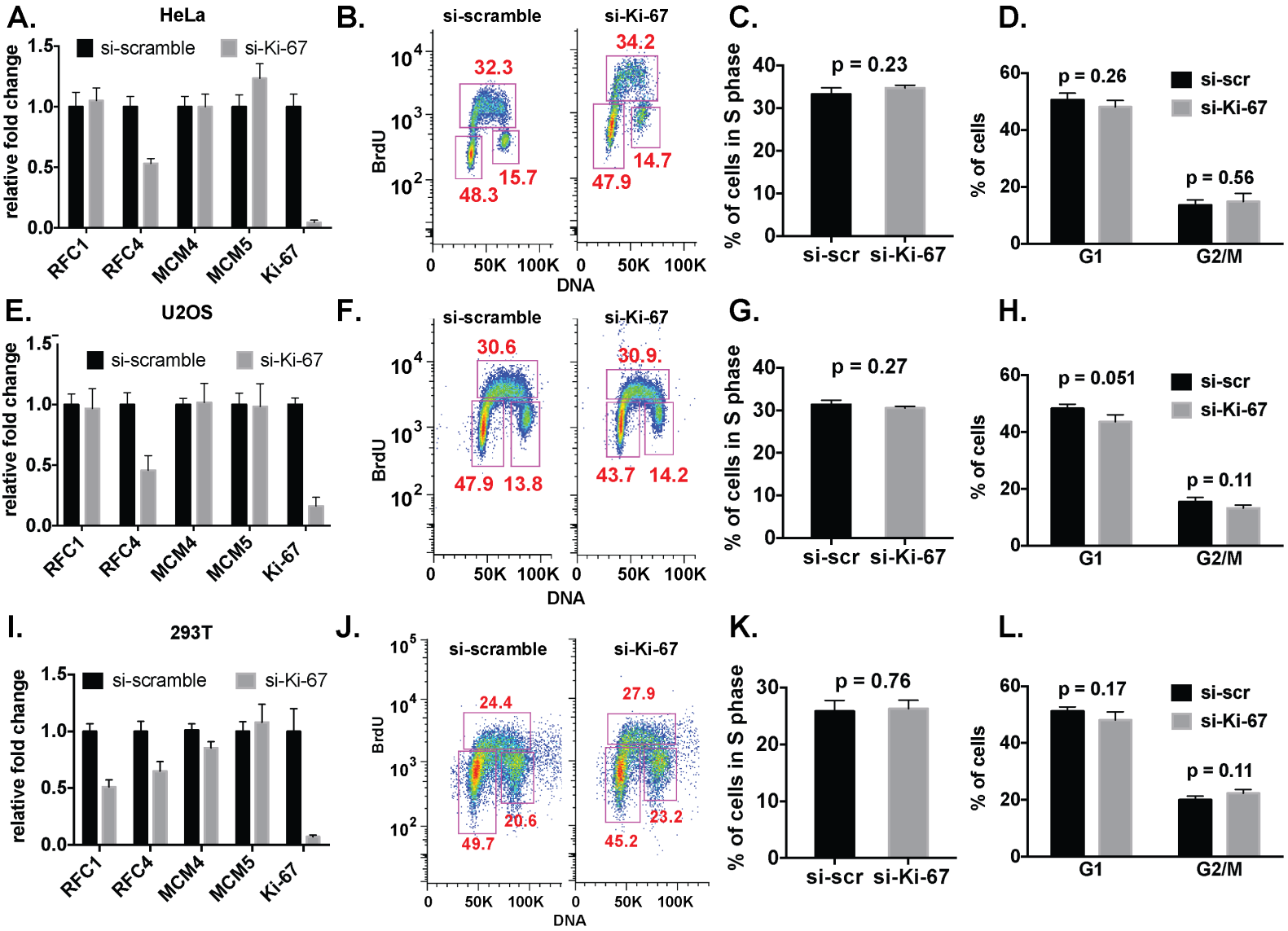
A.
HeLa
si-scramble
si-Ki-67
relative fold change
1.5
1.0
0.5
0.0
RFC1
RFC4
MCM4
MCM5
Ki-67
B.
si-scramble
si-Ki-67
BrdU
DNA
32.3
48.3
15.7
34.2
47.9
14.7
0
50K
100K
C.
% of cells in S phase
p = 0.23
si-scr
si-Ki-67
D.
% of cells
p = 0.26
p = 0.56
si-scr
si-Ki-67
G1
G2/M
E.
U2OS
F.
30.6
47.9
13.8
30.9
43.7
14.2
G.
p = 0.27
H.
p = 0.051
p = 0.11
I.
293T
J.
24.4
49.7
20.6
27.9
45.2
23.2
K.
p = 0.76
L.
p = 0.17
p = 0.11

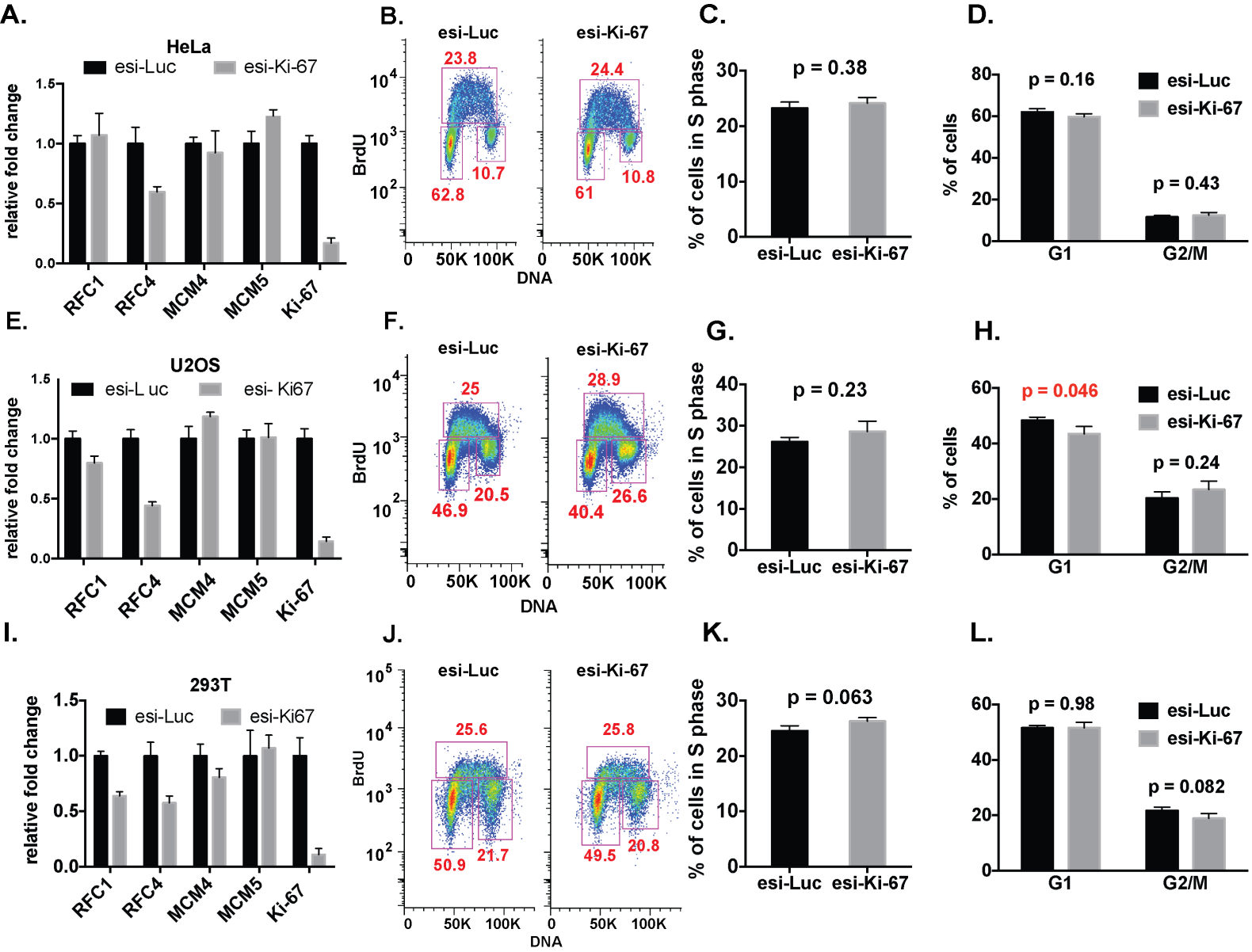
A.
HeLa
esi-Luc
esi-Ki-67
relative fold change
1.5
1.0
0.5
0.0
RFC1
RFC4
MCM4
MCM5
Ki-67
B.
esi-Luc
esi-Ki-67
23.8
10.7
62.8
24.4
10.8
61
BrdU
DNA
0
50K
100K
C.
p = 0.38
% of cells in S phase
esi-Luc
esi-Ki-67
D.
p = 0.16
p = 0.43
% of cells
G1
G2/M
E.
U2OS
esi-L uc
esi- Ki67
F.
25
20.5
46.9
28.9
26.6
40.4
G.
p = 0.23
H.
p = 0.046
p = 0.24
I.
293T
esi-Ki67
J.
25.6
21.7
50.9
25.8
20.8
49.5
K.
p = 0.063
L.
p = 0.98
p = 0.082

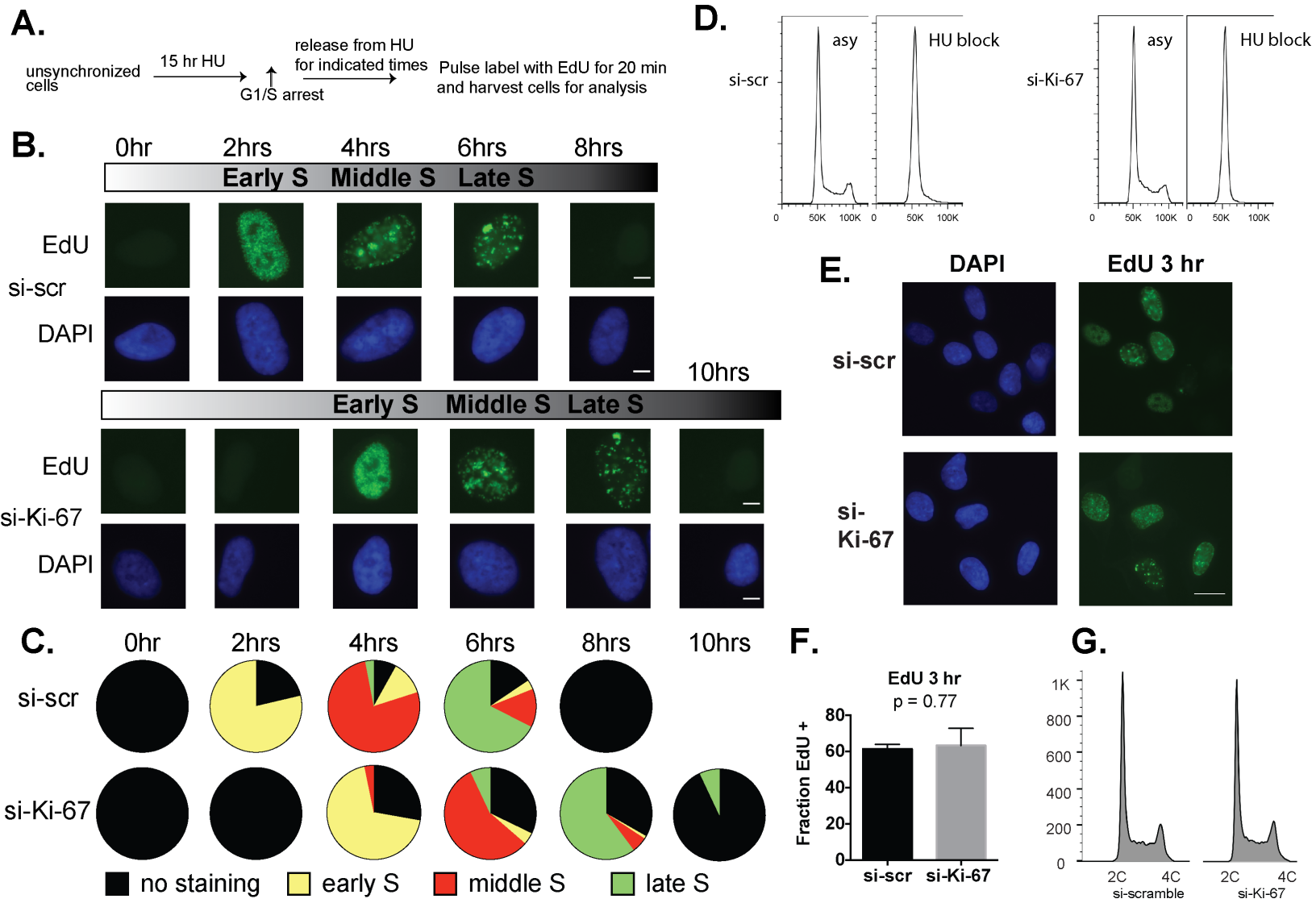
A.
unsynchronized cells
15 hr HU
G1/S arrest
release from HU for indicated times
Pulse label with EdU for 20 min and harvest cells for analysis
B.
0hr
2hrs
4hrs
6hrs
8hrs
10hrs
Early S
Middle S
Late S
EdU
si-scr
si-Ki-67
DAPI
C.
no staining
early S
middle S
late S
D.
asy
HU block
si-scr
si-Ki-67
0
50K
100K
E.
DAPI
EdU 3 hr
si-scr
si-Ki-67
F.
EdU 3 hr
p = 0.77
Fraction EdU +
80
60
40
20
0
si-scr
si-Ki-67
G.
1K
800
600
400
200
0
2C
4C
si-scramble
si-Ki-67

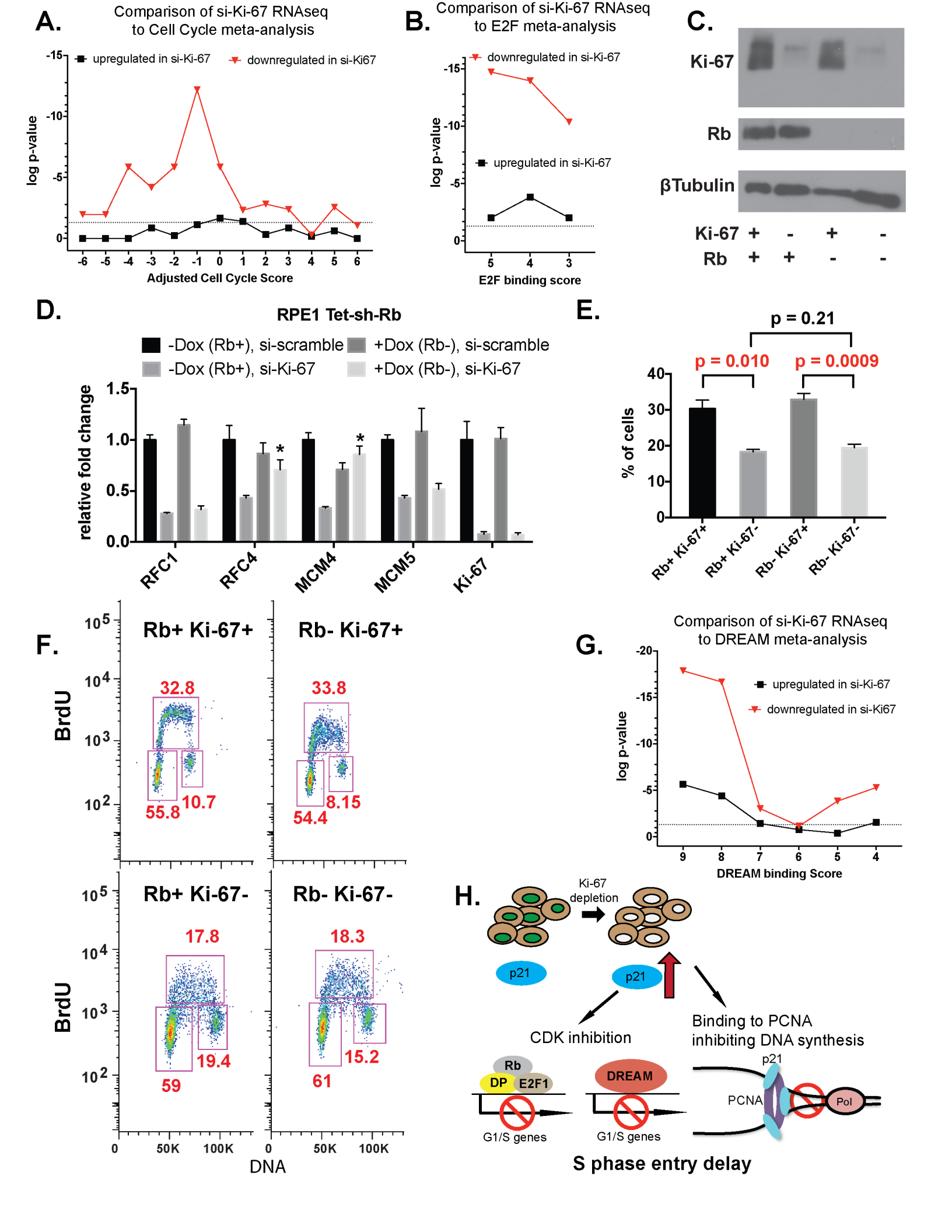
A.
Comparison of si-Ki-67 RNAseq to Cell Cycle meta-analysis
upregulated in si-Ki-67
downregulated in si-Ki67
log p-value
Adjusted Cell Cycle Score
B.
Comparison of si-Ki-67 RNAseq to E2F meta-analysis
downregulated in si-Ki-67
upregulated in si-Ki-67
log p-value
E2F binding score
C.
Ki-67
Rb
βTubulin
Ki-67 + - + -
Rb + + - -
D.
RPE1 Tet-sh-Rb
-Dox (Rb+), si-scramble
+Dox (Rb-), si-scramble
-Dox (Rb+), si-Ki-67
+Dox (Rb-), si-Ki-67
relative fold change
RFC1
RFC4
MCM4
MCM5
Ki-67
E.
p = 0.21
p = 0.010
p = 0.0009
% of cells
Rb+ Ki-67+
Rb+ Ki-67-
Rb- Ki-67+
Rb- Ki-67-
F.
Rb+ Ki-67+
Rb- Ki-67+
Rb+ Ki-67-
Rb- Ki-67-
BrdU
DNA
32.8
55.8
10.7
33.8
54.4
8.15
17.8
59
19.4
18.3
61
15.2
G.
Comparison of si-Ki-67 RNAseq to DREAM meta-analysis
upregulated in si-Ki-67
downregulated in si-Ki67
log p-value
DREAM binding Score
H.
Ki-67 depletion
p21
CDK inhibition
Binding to PCNA inhibiting DNA synthesis
Rb
DP
E2F1
DREAM
PCNA
Pol
G1/S genes
S phase entry delay

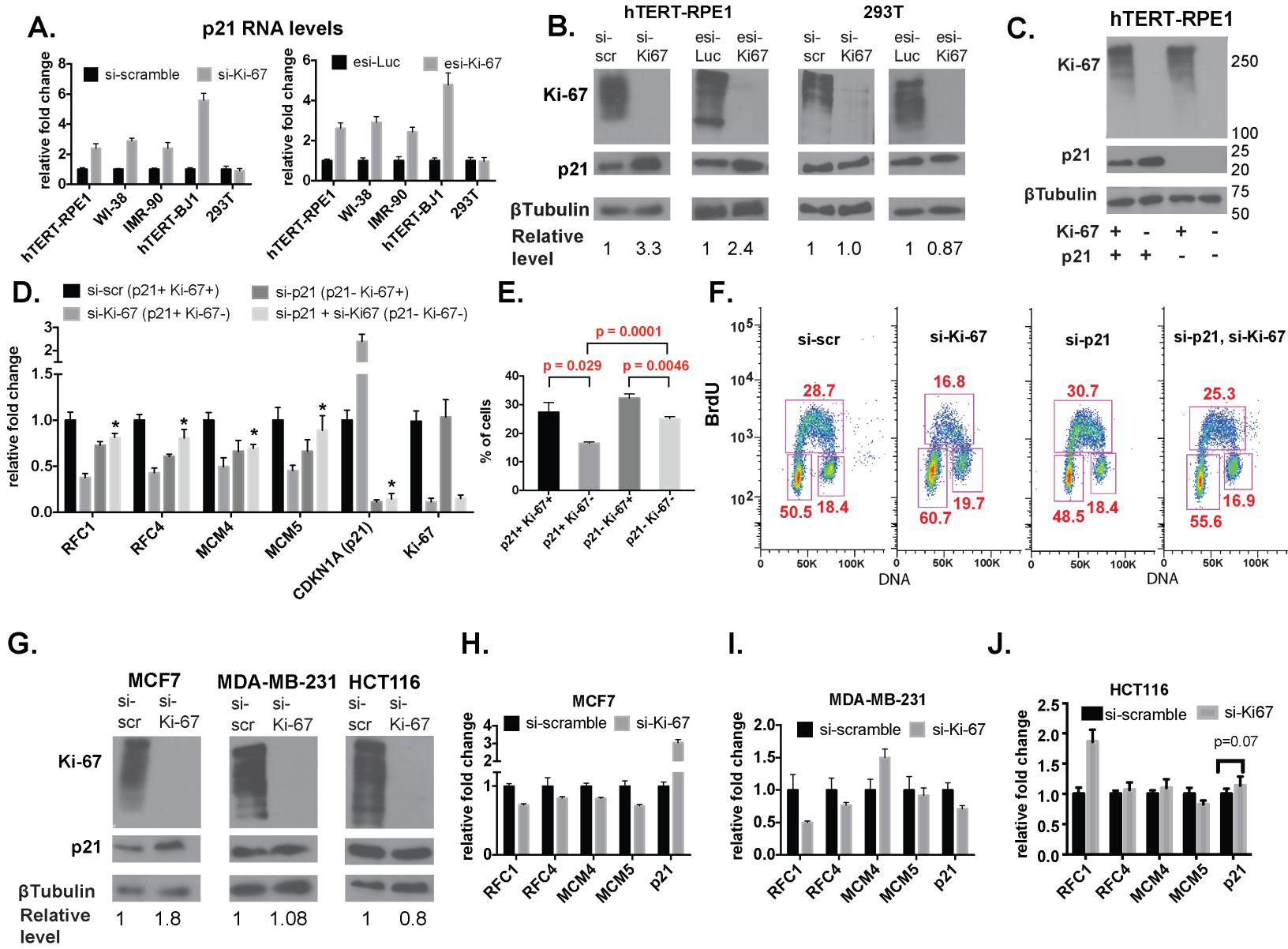
A.
p21 RNA levels
si-scramble
si-Ki-67
relative fold change
hTERT-RPE1
WI-38
IMR-90
hTERT-BJ1
293T
esi-Luc
esi-Ki-67
B.
hTERT-RPE1
293T
si-scr
si-Ki67
esi-Luc
esi-Ki67
Ki-67
p21
βTubulin
Relative level
1 3.3
1 2.4
1 1.0
1 0.87
C.
hTERT-RPE1
Ki-67
p21
βTubulin
250
100
25
20
75
50
Ki-67 + - + -
p21 + + - -
D.
si-scr (p21+ Ki-67+)
si-Ki-67 (p21+ Ki-67-)
si-p21 (p21- Ki-67+)
si-p21 + si-Ki67 (p21- Ki-67-)
relative fold change
RFC1
RFC4
MCM4
MCM5
CDKN1A (p21)
Ki-67
E.
p = 0.0001
p = 0.029
p = 0.0046
% of cells
p21+ Ki-67+
p21+ Ki-67-
p21- Ki-67+
p21- Ki-67-
F.
si-scr
si-Ki-67
si-p21
si-p21, si-Ki-67
BrdU
DNA
28.7
50.5
18.4
16.8
60.7
19.7
30.7
48.5
18.4
25.3
55.6
16.9
G.
MCF7
MDA-MB-231
HCT116
si-scr
si-Ki-67
Ki-67
p21
βTubulin
Relative level
1 1.8
1 1.08
1 0.8
H.
MCF7
si-scramble
si-Ki-67
relative fold change
RFC1
RFC4
MCM4
MCM5
p21
I.
MDA-MB-231
si-scramble
si-Ki-67
relative fold change
RFC1
RFC4
MCM4
MCM5
p21
J.
HCT116
si-scramble
si-Ki67
p=0.07
relative fold change
RFC1
RFC4
MCM4
MCM5
p21

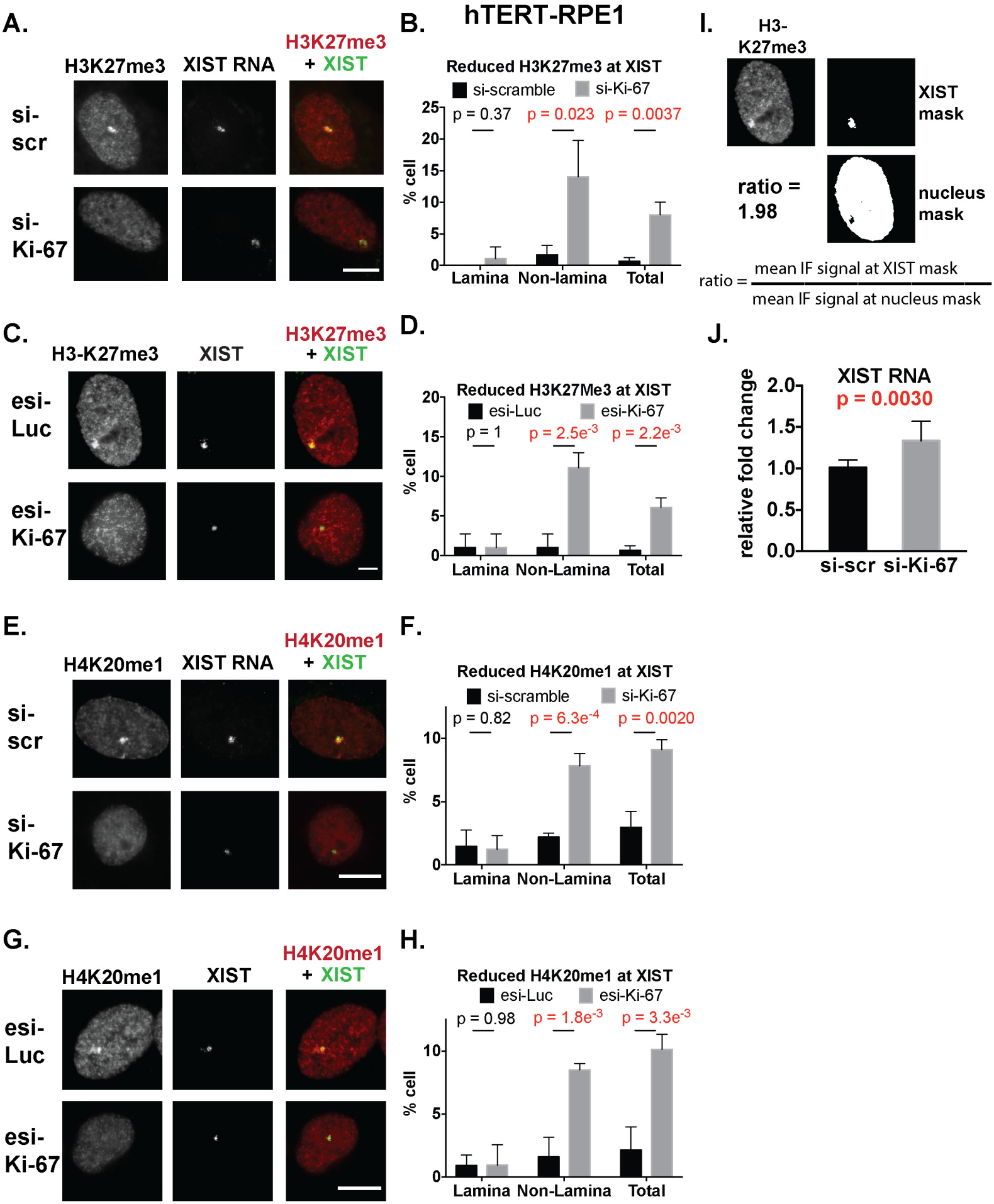
A.
H3K27me3
XIST RNA
H3K27me3 + XIST
si-scr
si-Ki-67
B.
hTERT-RPE1
Reduced H3K27me3 at XIST
si-scramble
si-Ki-67
p = 0.37
p = 0.023
p = 0.0037
% cell
Lamina
Non-lamina
Total
I.
H3-K27me3
XIST mask
ratio = 1.98
nucleus mask
ratio = mean IF signal at XIST mask / mean IF signal at nucleus mask
C.
H3-K27me3
XIST
H3K27me3 + XIST
esi-Luc
esi-Ki-67
D.
Reduced H3K27Me3 at XIST
esi-Luc
esi-Ki-67
p = 1
p = 2.5e-3
p = 2.2e-3
% cell
Lamina
Non-Lamina
Total
J.
XIST RNA
p = 0.0030
relative fold change
si-scr
si-Ki-67
E.
H4K20me1
XIST RNA
H4K20me1 + XIST
si-scr
si-Ki-67
F.
Reduced H4K20me1 at XIST
si-scramble
si-Ki-67
p = 0.82
p = 6.3e-4
p = 0.0020
% cell
Lamina
Non-Lamina
Total
G.
H4K20me1
XIST
H4K20me1 + XIST
esi-Luc
esi-Ki-67
H.
Reduced H4K20me1 at XIST
esi-Luc
esi-Ki-67
p = 0.98
p = 1.8e-3
p = 3.3e-3
% cell
Lamina
Non-Lamina
Total

293T

A.

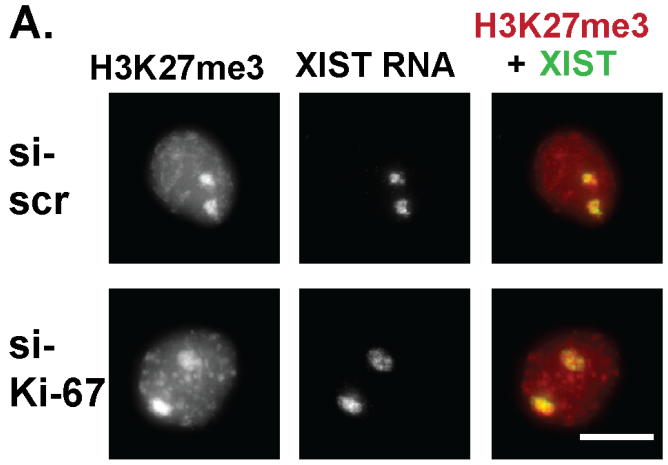

B.

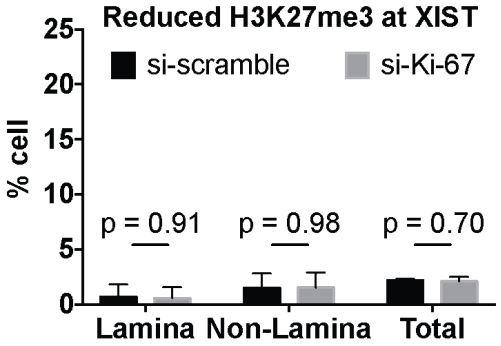

C.

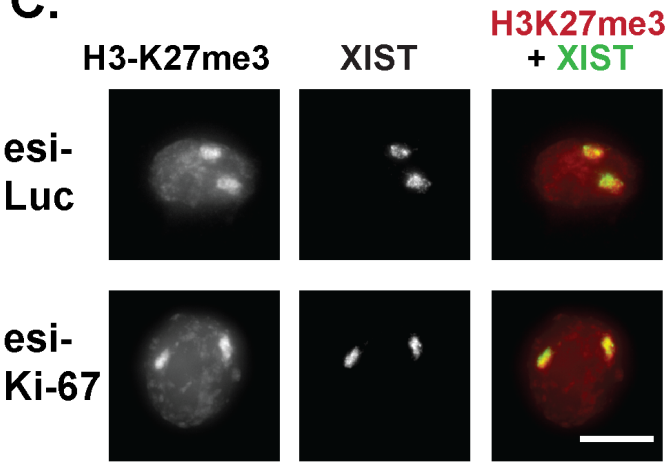

D.

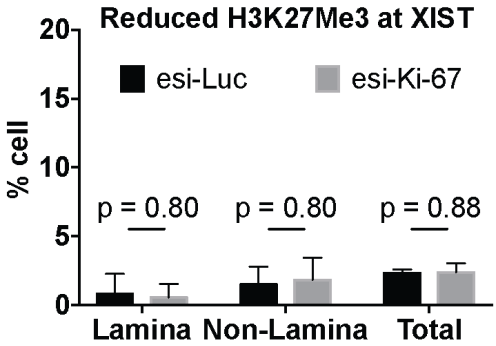

E.

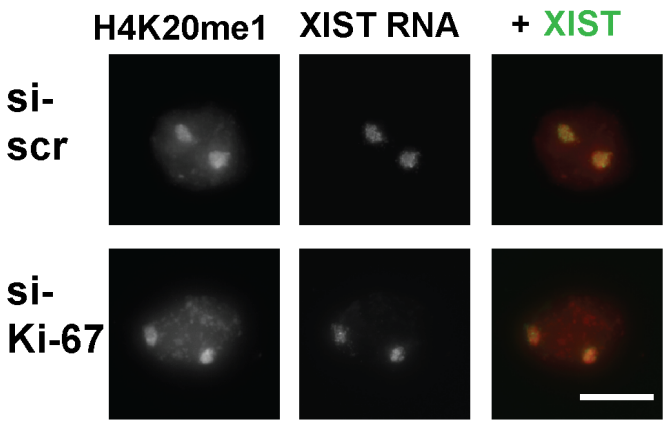

F.

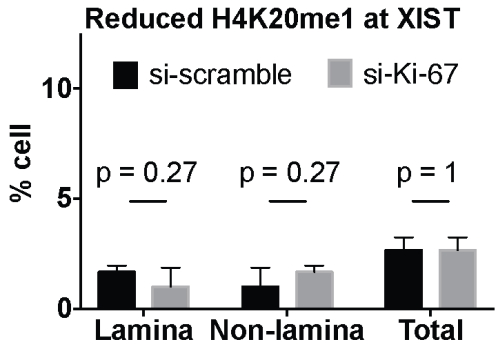

G.

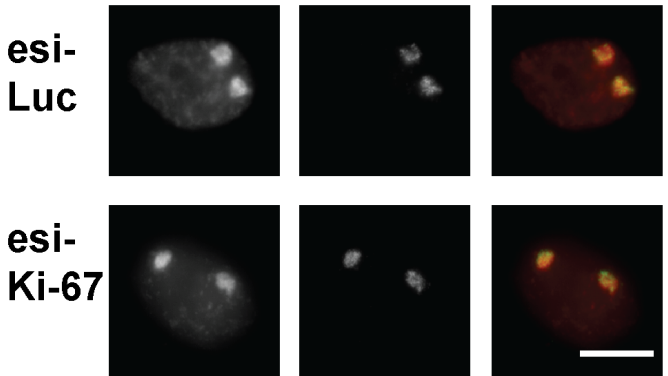

H.

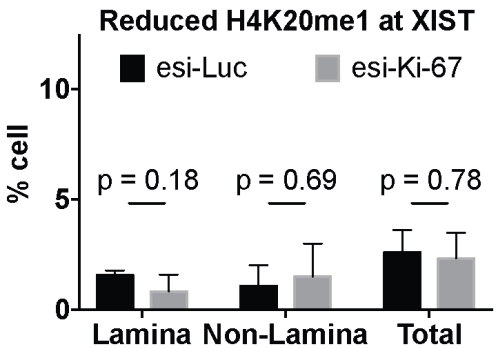

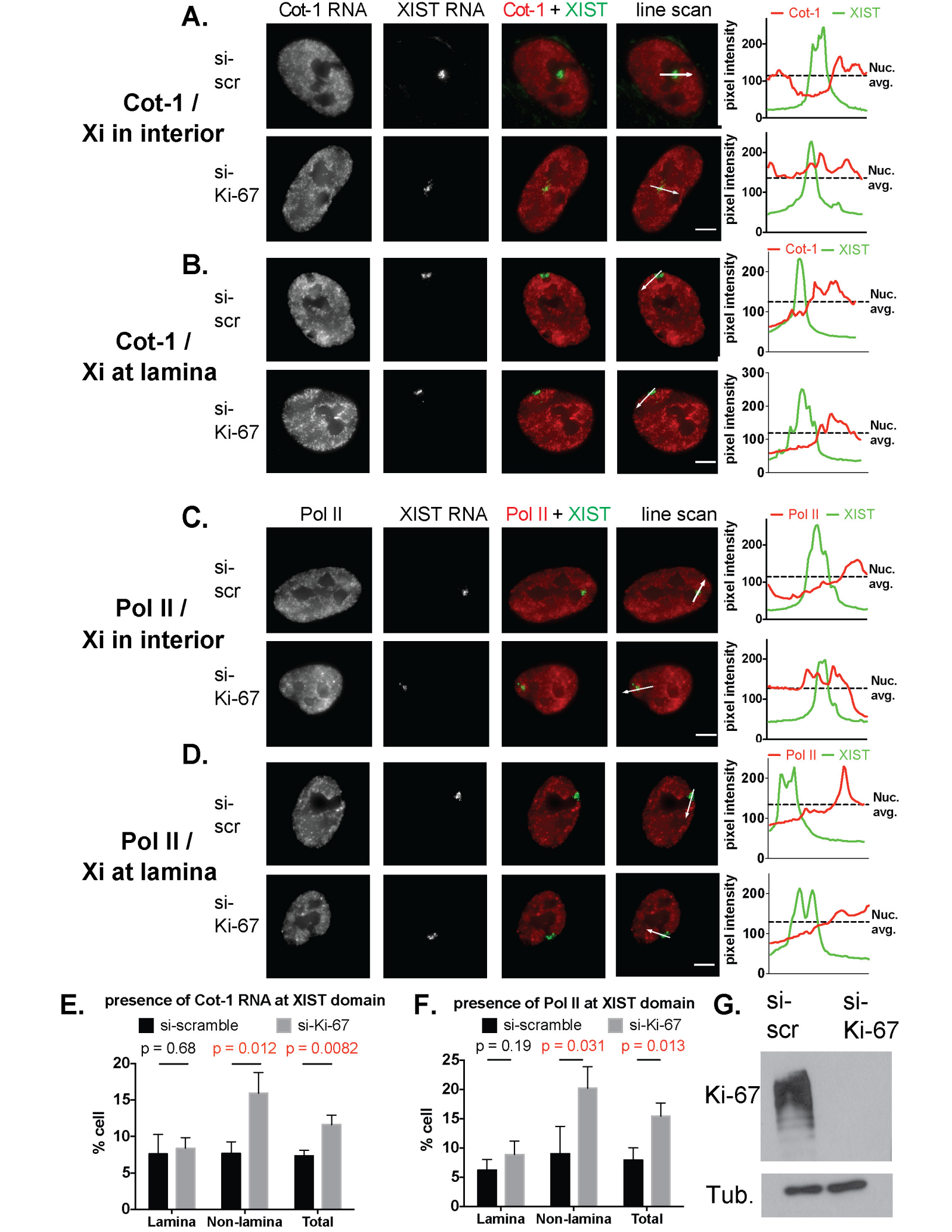
A.
Cot-1 RNA
XIST RNA
Cot-1 + XIST
line scan
Cot-1 / Xi in interior
si-scr
si-Ki-67
Cot-1
XIST
pixel intensity
Nuc. avg.
B.
Cot-1 / Xi at lamina
C.
Pol II
Pol II + XIST
Pol II / Xi in interior
D.
Pol II / Xi at lamina
E.
presence of Cot-1 RNA at XIST domain
si-scramble
si-Ki-67
p = 0.68
p = 0.012
p = 0.0082
% cell
Lamina
Non-lamina
Total
F.
presence of Pol II at XIST domain
p = 0.19
p = 0.031
p = 0.013
G.
si-scr
si-Ki-67
Ki-67
Tub.

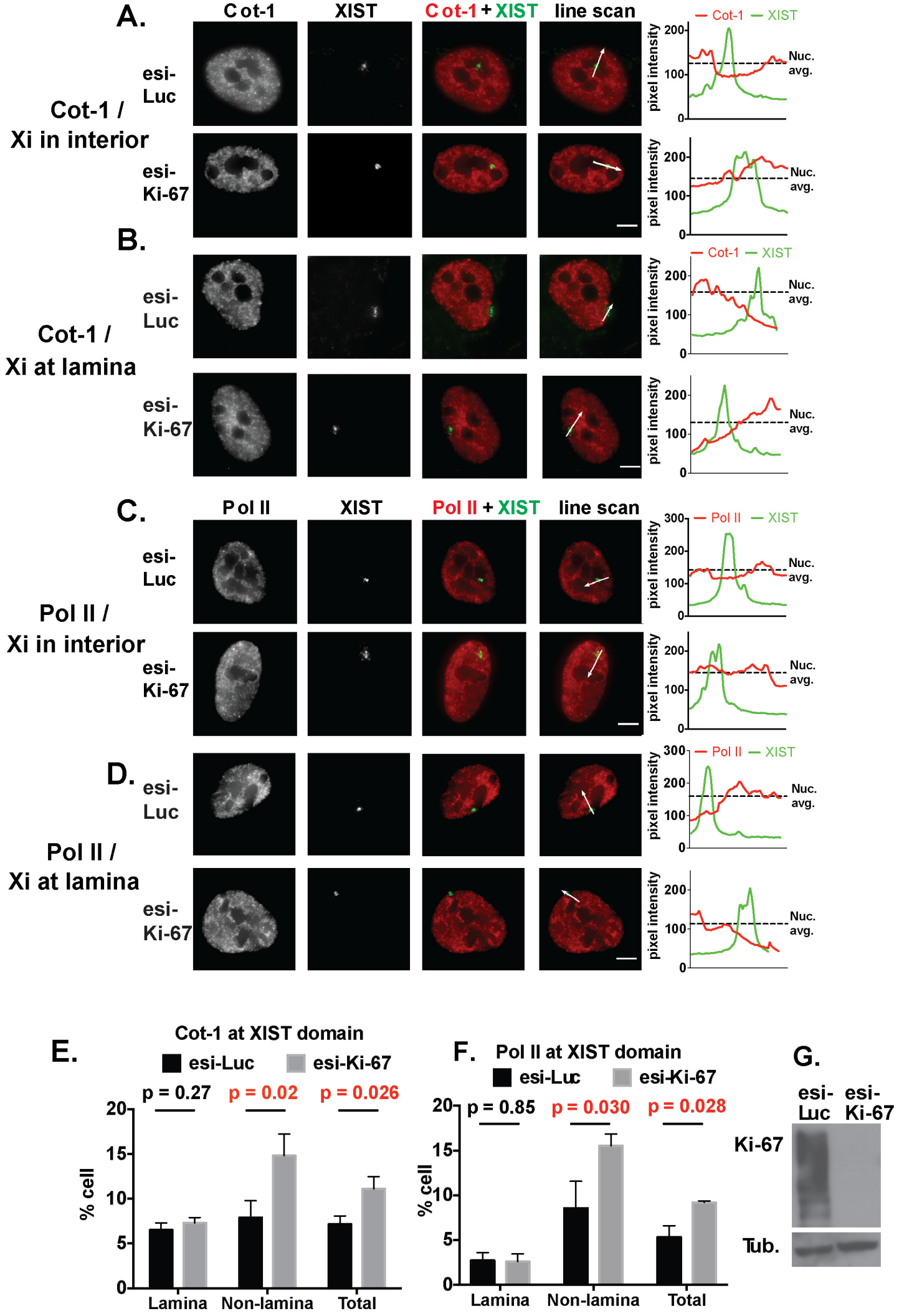
A.
Cot-1
XIST
Cot-1 + XIST
line scan
Cot-1 / Xi in interior
esi-Luc
esi-Ki-67
pixel intensity
Nuc. avg.
B.
Cot-1 / Xi at lamina
C.
Pol II
Pol II + XIST
Pol II / Xi in interior
D.
Pol II / Xi at lamina
E.
Cot-1 at XIST domain
esi-Luc
esi-Ki-67
p = 0.27
p = 0.02
p = 0.026
% cell
Lamina
Non-lamina
Total
F.
Pol II at XIST domain
p = 0.85
p = 0.030
p = 0.028
G.
Ki-67
Tub.

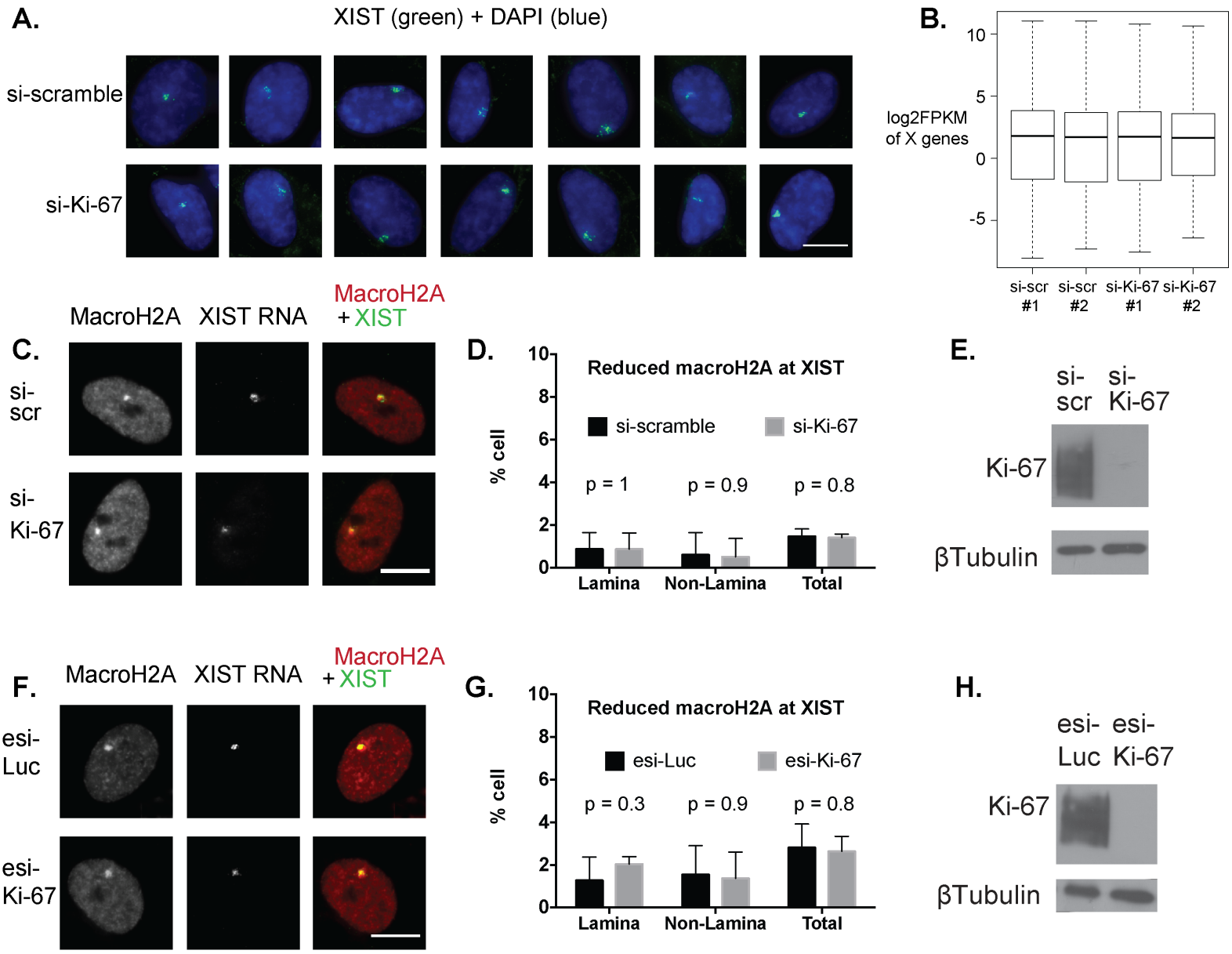
A.
XIST (green) + DAPI (blue)
si-scramble
si-Ki-67
B.
log2FPKM of X genes
10
5
0
-5
si-scr #1
si-scr #2
si-Ki-67 #1
si-Ki-67 #2
C.
MacroH2A
XIST RNA
MacroH2A + XIST
si-scr
si-Ki-67
D.
Reduced macroH2A at XIST
% cell
si-scramble
si-Ki-67
p = 1
p = 0.9
p = 0.8
Lamina
Non-Lamina
Total
E.
si-scr
si-Ki-67
Ki-67
βTubulin
F.
MacroH2A
XIST RNA
MacroH2A + XIST
esi-Luc
esi-Ki-67
G.
Reduced macroH2A at XIST
% cell
esi-Luc
esi-Ki-67
p = 0.3
p = 0.9
p = 0.8
Lamina
Non-Lamina
Total
H.
esi-Luc
esi-Ki-67
Ki-67
βTubulin

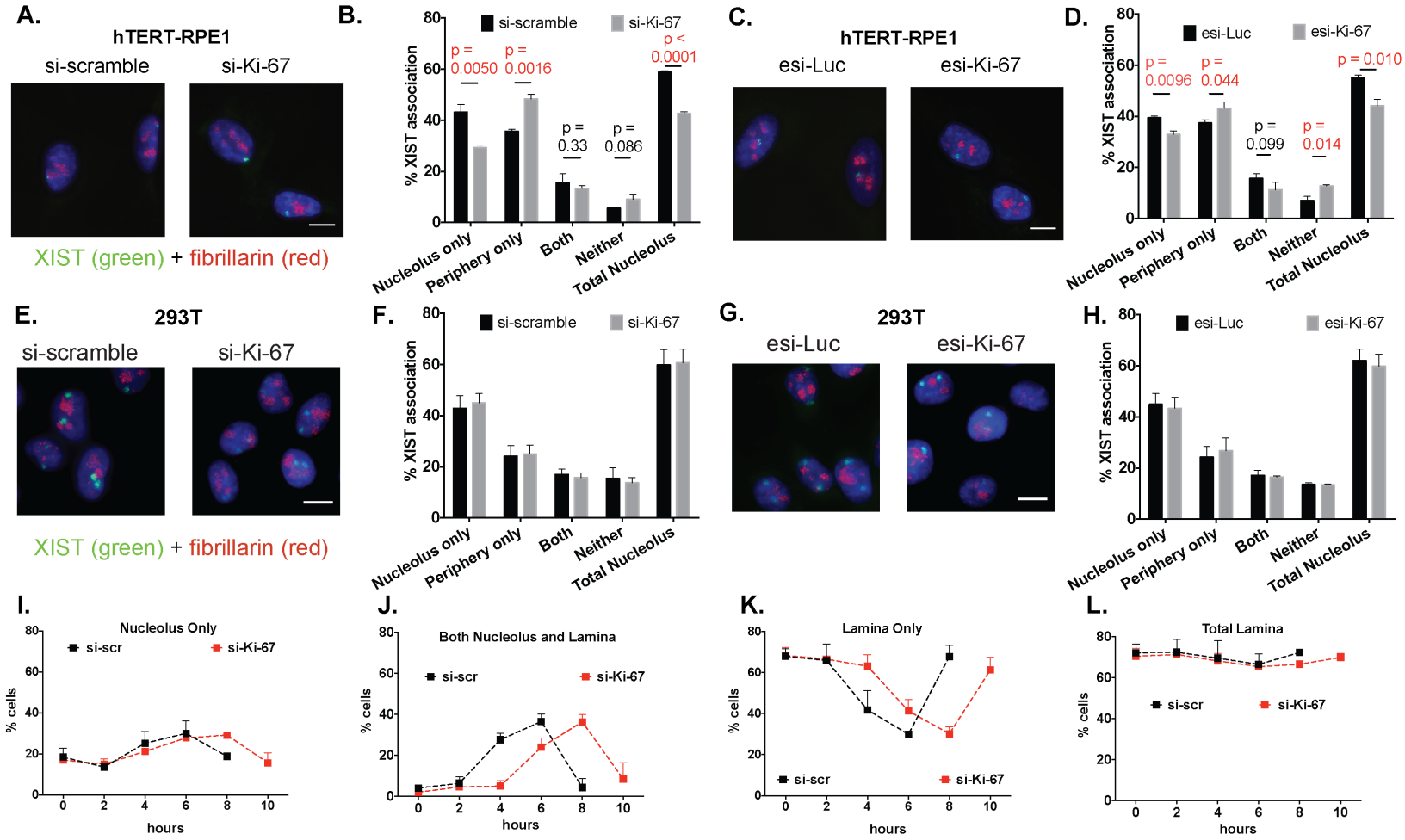
A.
hTERT-RPE1
si-scramble
si-Ki-67
XIST (green) + fibrillarin (red)
B.
si-scramble
si-Ki-67
% XIST association
p = 0.0050
p = 0.0016
p = 0.33
p = 0.086
p < 0.0001
Nucleolus only
Periphery only
Both
Neither
Total Nucleolus
C.
hTERT-RPE1
esi-Luc
esi-Ki-67
D.
esi-Luc
esi-Ki-67
% XIST association
p = 0.0096
p = 0.044
p = 0.099
p = 0.014
p = 0.010
Nucleolus only
Periphery only
Both
Neither
Total Nucleolus
E.
293T
si-scramble
si-Ki-67
XIST (green) + fibrillarin (red)
F.
si-scramble
si-Ki-67
% XIST association
Nucleolus only
Periphery only
Both
Neither
Total Nucleolus
G.
293T
esi-Luc
esi-Ki-67
H.
esi-Luc
esi-Ki-67
% XIST association
Nucleolus only
Periphery only
Both
Neither
Total Nucleolus
I.
Nucleolus Only
si-scr
si-Ki-67
% cells
hours
J.
Both Nucleolus and Lamina
si-scr
si-Ki-67
% cells
hours
K.
Lamina Only
si-scr
si-Ki-67
% cells
hours
L.
Total Lamina
si-scr
si-Ki-67
% cells
hours